Earth and Planetary Science Letters 508 (2019) 41–50

Contents lists available at ScienceDirect

Earth and Planetary Science Letters

www.elsevier.com/locate/epsl

Seafloor weathering and the oxygen isotope ratio in seawater: Insight from whole-rock $\delta^{18}O$ and carbonate $\delta^{18}O$ and Δ_{47} from the Troodos ophiolite

L.A. Coogan [a,*], M. Daëron [b], K.M. Gillis [a]

[a] School of Earth and Ocean Sciences, University of Victoria, Victoria, V8P 5C2, Canada
[b] CNRS/LSCE, Batiment 12 – Avenue de la Terrasse, 91198 Gif-sur-Yvette, France

ARTICLE INFO

Article history:
Received 11 July 2018
Received in revised form 8 November 2018
Accepted 16 December 2018
Available online xxxx
Editor: L. Derry

Keywords:
O-isotopes in seawater
seafloor weathering
long-term C-cycle

ABSTRACT

The controls on, and history of, the oxygen isotope ratio in seawater continue to be debated after many decades of research with the lack of consensus in large part reflecting uncertainty in the role of hydrothermal exchange between seawater and the oceanic crust. We have investigated this using new carbonate Δ_{47} and $\delta^{18}O$ data, and whole-rock O-isotope data, for samples from the lava section of the Troodos ophiolite. Carbonate data confirm that fluid-to-rock ratios in the upper lavas during off-axis hydrothermal circulation are generally sufficiently large that both the fluid $\delta^{18}O$ and temperature are similar to those of bottom water. However, some samples require more complicated interpretations that could reflect changes in the rate of calcite formation. Whole-rock data indicate that O-isotope exchange in the lavas is directly linked to the major element exchange that leads to alkalinity production (i.e., CO_2 consumption) and both are dependent on bottom water temperature. This means that the O-isotopic composition of seawater is linked to the long-term C-cycle. The data are used to parameterise a simple model of the evolution of the O-isotopic composition of seawater driven by changes in solid earth CO_2 degassing. Alkalinity balance links the total extent of weathering of the continents and seafloor, which are sinks for high $\delta^{18}O$ material, to CO_2 degassing rate and surface temperature. The modelling suggests that if solid earth CO_2 degassing and the rate of formation of oceanic crust are linked, the O-isotopic composition of the ocean (including any ice sheets) is unlikely to have varied more than $\pm 1‰$ over the Phanerozoic.

1. Introduction

The oxygen isotope composition of seawater ($\delta^{18}O_{SW}$) provides important insight into the fluid–rock interactions, both on the continents and at the bottom of the oceans, that control important aspects of ocean chemistry (e.g. Muehlenbachs and Clayton, 1976; Jaffrés et al., 2007). Continental weathering leads to O-isotope fractionation between the weathering products and associated fluids that ultimately return to the ocean (e.g. Savin and Epstein, 1970). Likewise, seafloor hydrothermal systems fractionate O-isotopes between the secondary minerals and modified seawater (Gregory and Taylor, 1981; Alt et al., 1986). Precipitation of chemical sediments and diagenetic phases are also associated with O-isotope fractionation. Because the processes that control the O-isotopic composition of the ocean are important for many long-term element cycles in the ocean, a quantitative understanding of the controls on the O-isotope composition of seawater, and how this has changed over Earth history, is of fundamental importance to our understanding of the Earth system.

Despite decades of research there is an ongoing controversy about whether $\delta^{18}O_{SW}$ has changed substantially, or remained almost constant, over Earth history. On one hand, the $\delta^{18}O$ of carbonates and cherts are generally isotopically lighter the older they are (Perry, 1967; Fritz, 1971), with early Phanerozoic and Archean carbonates ~6 to 8‰ and ~15‰ lighter than modern carbonates, respectively (e.g. Veizer and Prokoph, 2015; Shields and Veizer, 2002; Jaffrés et al., 2007). This has been interpreted as indicating similarly light palaeoseawater (Perry, 1967; Walker and Lohmann, 1989; Veizer et al., 1999; Wallmann, 2004; Kasting et al., 2006; Jaffrés et al., 2007; Veizer and Prokoph, 2015). Alternatively, it has been argued that the formation of low $\delta^{18}O$ secondary minerals in high-temperature, on-axis, seafloor hydrothermal systems, and high $\delta^{18}O$ secondary minerals in low-temperature, off-axis, seafloor hydrothermal systems tends to force $\delta^{18}O_{SW}$ towards be-

* Corresponding author.
E-mail address: lacoogan@uvic.ca (L.A. Coogan).

https://doi.org/10.1016/j.epsl.2018.12.014
0012-821X/

ing ~6‰ lighter than oceanic crust (e.g. Muehlenbachs, 1998). Since the $\delta^{18}O$ of the mantle has remained almost constant over time, the implication of this model is that the same must be true for seawater (Muehlenbachs and Clayton, 1976; Gregory and Taylor, 1981; Muehlenbachs, 1998; Turchyn et al., 2013). Recently, clumped isotope measurements of sedimentary carbonates have provided independent evidence that $\delta^{18}O_{SW}$ has not changed substantially over the Phanerozoic (Came et al., 2007; Cummins et al., 2014; Finnegan et al., 2011; Henkes et al., 2018; Ryb and Eiler, 2018) however the interpretation of these data have been questioned (Veizer and Prokoph, 2015). Resolutions to this controversy range from explaining the carbonate and chert $\delta^{18}O$ record as reflecting high paleoseawater temperatures and/or post-depositional modification through to postulating significant changes in how oceanic hydrothermal systems operate (e.g. Muehlenbachs, 1998; Gregory and Taylor, 1981; Kasting et al., 2006; Jaffrés et al., 2007).

Irrespective of whether authors conclude that $\delta^{18}O_{SW}$ has remained nearly constant or changed dramatically, it is generally accepted that oceanic hydrothermal processes are key in controlling $\delta^{18}O_{SW}$ (e.g. Muehlenbachs, 1998; Lécuyer and Allemand, 1999; Gregory and Taylor, 1981; Kasting et al., 2006; Jaffrés et al., 2007). A number of recent studies have suggested that $\delta^{18}O_{SW}$ increased ~6‰ over the Phanerozoic and that this was largely due to a decrease in the extent of low-temperature alteration of the upper oceanic crust (Wallmann, 2004; Kasting et al., 2006; Jaffrés et al., 2007). In this model increased abyssal sedimentation starting in the early Phanerozoic is hypothesised to have reduced the extent of off-axis hydrothermal alteration of the lavas decreasing the magnitude of this high $\delta^{18}O$ sink. Here we present new carbonate (Δ_{47} and $\delta^{18}O$) and whole-rock ($\delta^{18}O$) analyses of seafloor lavas from the Troodos ophiolite. These data, along with compiled data, are used to guide the construction and calibration of a simple model of the controls on $\delta^{18}O_{SW}$. The model shows that coupling between the C-cycle and $\delta^{18}O_{SW}$ make a 6–8‰ change in $\delta^{18}O_{SW}$ over the Phanerozoic unlikely.

2. Oxygen isotope exchange between the ocean and the oceanic crust

Oxygen-isotope exchange between the ocean and oceanic crust occurs under very different conditions in on- and off-axis regions (Fig. 1). On-axis hydrothermal circulation is driven by the cooling of magma chambers and plutonic rocks, with larger fluid fluxes in the higher permeability dikes than in the underlying, lower permeability, plutonic rocks. Temperatures of fluid–rock interaction in the dikes and plutonic rocks are typically 350–750 °C leading to the formation of secondary minerals that are predicted to have $^{18}O/^{16}O$ ratios similar to that of the fluid they grew from ($1000\ln(\alpha_{r/w}) \sim 0 \pm 2$‰, where $\alpha_{r/w}$ is the $^{18}O/^{16}O$ fractionation factor between rock and water). High-temperatures and hydrous conditions are expected to lead to a close approach to equilibrium O-isotope exchange. This means that for the modern system the $\delta^{18}O$ of dikes and plutonic rocks (initial $\delta^{18}O_{SMOW}$ ~5.7‰) decrease slightly during on-axis, high-temperature, hydrothermal alteration (Fig. 2; Alt et al., 1986; Gregory and Taylor, 1981). The average dike from the modern ocean basin ($\delta^{18}O_{SMOW} = 4.5$‰; standard error = 0.06; $n = 219$) is slightly isotopically lighter than the average plutonic rock ($\delta^{18}O_{SMOW} = 5.1$‰; standard error = 0.08; $n = 315$), largely because the higher permeability in the dikes leads to higher water-to-rock ratios (~1 versus <1; e.g., Alt et al., 1986; Kirchner and Gillis, 2012). A more limited dataset from the Troodos ophiolite gives a very similar result (Fig. 2), consistent with high-temperature alteration of the dikes and plutonics operating under similar conditions as in modern crust.

Fluid-flow in the off-axis is driven by the cooling of the oceanic lithosphere and is focused in the high permeability lavas (upper ~500 m of the crust) where water-to-rock ratios are about three orders of magnitude higher than in on-axis systems (Fig. 1; e.g., Coogan and Gillis, 2018a). Because fluid–rock reactions occur at low temperatures the newly formed minerals have O-isotope ratios significantly higher than the fluids they grow from ($1000\ln(\alpha_{r/w}) \sim 30$; Fig. S1), however, recrystallisation is generally incomplete (i.e. the rocks are mixtures of fresh igneous phases and secondary minerals). Compiled whole-rock O-isotope compositions of seafloor lavas from modern ocean crust are heavier than fresh rocks (Fig. 2). They also have more variable O-isotope compositions than dikes and plutonic rocks, due to the more heterogeneous distribution of low-temperature alteration. Strikingly, lavas from Mesozoic age oceanic crust, altered when bottom water temperatures were relatively high (~15 °C; e.g., Friedrich et al., 2012), commonly have substantially heavier O-isotope compositions than lavas altered under cooler bottom water conditions (≤5 °C) in the late Cenozoic (Fig. 2). A Kolmogorov–Smirnov test of the difference in data distribution between the Mesozoic (arithmetic mean $\delta^{18}O_{SMOW} = 10.6$‰; standard error = 0.3‰; geometric mean = 9.9‰; $n = 210$) and late Cenozoic samples (arithmetic mean $\delta^{18}O = 7.0$‰; standard error = 0.1‰; geometric mean = 6.9‰; $n = 151$) confirms that the observed difference in $\delta^{18}O$ distribution is statistically significant ($p = 10^{-22}$). The skewed distribution of the O-isotopic composition of >75 Myr old lavas is what would be expected if samples have been variably, and incompletely, replaced by a high $\delta^{18}O$ secondary mineral assemblage. This difference in the O-isotope composition of altered lavas (but not dikes or plutonics) as a function of their age cannot simply be a result of progressive ageing of the crust because most alteration in the lavas occurs in the first 20 Myrs after crustal accretion (e.g. Staudigel and Hart, 1985; Coogan and Gillis, 2018a). Nor can this be explained by the temperature dependence of $\alpha_{r/w}$, because cooler conditions lead to larger, not smaller, isotopic fractionations. Instead, the most likely explanation of the higher $\delta^{18}O$ of Mesozoic

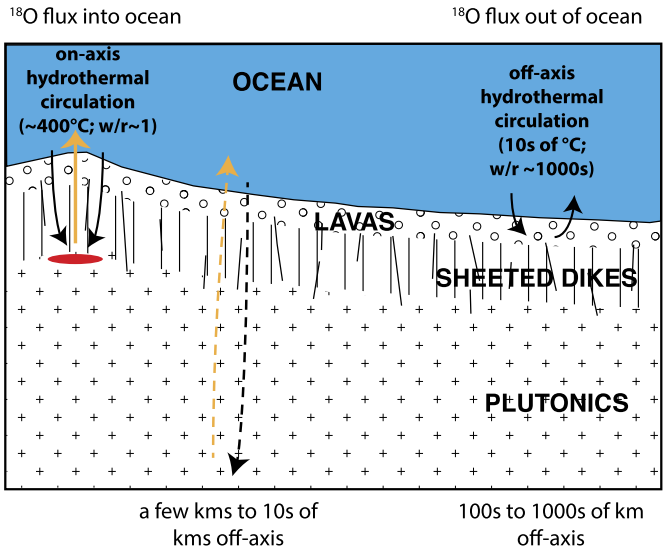

Fig. 1. Schematic illustration (not to scale) of the processes in the oceanic crust that modify $\delta^{18}O_{SW}$. Reactions associated with on-axis hydrothermal circulation mainly occur in the sheeted dikes, where fluid flow is driven by the cooling of magma chambers (red ellipse in figure) and plutonic rocks with lesser fluid flow through the plutonics. For the modern system ($\delta^{18}O_{SW}$ ~0‰) these high-temperature reactions lead to the rocks becoming isotopically lighter relative to the fresh rocks (5.7‰). Off-axis hydrothermal circulation in the lava section of the crust, that occurs across the abyssal plains at low-temperatures, leads to the rocks becoming isotopically heavier. Fluid flow is shown as arrows; black = cool; yellow = hot; dashing indicates smaller, but less well known, fluid fluxes (in the plutonic section). (For interpretation of the colours in the figure(s), the reader is referred to the web version of this article.)

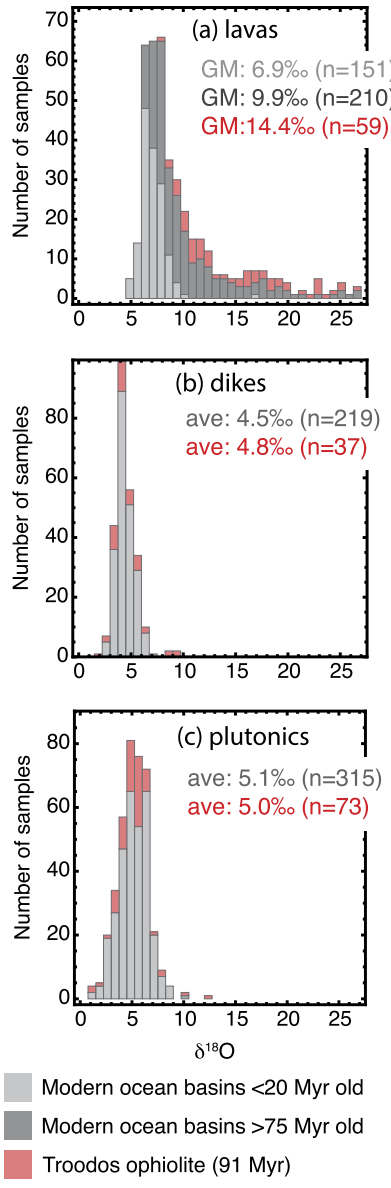

Fig. 2. Histograms of compiled and new (see later) O-isotope compositions of lavas (VSMOW), dikes and plutonic rocks from the modern ocean basins and the Troodos ophiolite. The data for dikes and plutonic rocks from the modern ocean basins are all from <20 Myr old crust and have very similar distributions to the same lithologies in the Cretaceous Troodos ophiolite. In contrast, there is a distinct difference between lava samples from young (<20 Myr) and old (>75 Myr) crust with the Troodos ophiolite samples being more similar to the older samples from the modern ocean basins. Because of the non-normal data distribution for lavas geometric means (GM) are given instead of arithmetic means (ave). Sources of data are listed in Supplementary Table S4.

than late Cenozoic lavas is that they underwent greater extents of fluid–rock reaction and O-isotope exchange due to the higher bottom water temperature increasing reaction rates.

3. Sample suite and analytical techniques

To further investigate the controls on O-isotope exchange between seawater and lavas during off-axis hydrothermal circulation we have studied a ~20 km wide section of lavas exposed on the northern flank of the Cretaceous Troodos ophiolite (Supplementary Fig. S2). Whole-rock samples were collected along four traverses through the lava section (Coogan et al., 2017; Coogan and Gillis, 2018b). Carbonates were collected from throughout the study area and come mainly from amygdales but occasionally from vugs and veins. Whole-rock samples are variably altered to mineral assemblages that include clays, zeolites, calcite, K-feldspar, celadonite, chalcedony and Fe-oxy-hydroxides (e.g. Gillis and Robinson, 1990; Coogan and Gillis, 2018b).

Forty-six whole rock lavas were analysed for O-isotopes (Table S1) at Western University following procedures reported by Polat et al. (2018). Analyses of an in-house quartz standard and a CO_2 gas standard gave $\delta^{18}O_{SMOW} = 11.44 \pm 0.27‰$ (1 standard deviation; SD; $n = 9$) and $10.19 \pm 0.03‰$ (1 SD; $n = 11$) relative to accepted values of 11.5‰ and 10.3‰. Three analyses of NBS28 (NIST RM 8546) run as an unknown gave $\delta^{18}O_{SMOW} = 9.61 \pm 0.02‰$ (1 SD) relative to the accepted value of $9.58 \pm 0.09‰$. The average standard deviation of replicate sample analyses was 0.39‰ ($n = 12$). The greater scatter in the sample than standard data suggests this reflects sample inhomogeneity. Strontium isotope ratios were also measured on samples not already analysed by Gillis et al. (2015) using identical procedures as in that study (Table S1).

Oxygen-isotope data for one hundred and eighty-four hand-picked carbonates from the study area are used to constrain the temperature of fluid–rock reaction (Table S2). Most were analysed at the University of British Columbia using a Delta PlusXL mass spectrometer in continuous flow mode as part of this project although some measurements come from previous studies and were performed in other laboratories (Gillis and Robinson, 1990; Gillis et al., 2015; all data are reported in Table S2). Duplicate analysis of the same powder gave results with an average absolute difference of 0.3‰. Complete sample duplication, including crushing and picking of different material from the same outcrop, led to a maximum difference of 1.4‰ (equivalent to ~7 °C).

Eleven samples were selected for clumped-isotope analysis (Table S3) based on their spanning the normal range of $\delta^{18}O$ (i.e. excluding samples with extreme $\delta^{18}O$; see Section 4.1 and Fig. 4) and the geographical distribution of the study area (Fig. S2). The Sr and Mg contents of these samples were determined using standard ICP-MS (University of Victoria) and their $^{87}Sr/^{86}Sr$ by TIMS (University of British Columbia; Weis et al., 2006). Carbonate clumped-isotope thermometry is based on the quantification of statistical anomalies in the abundance of doubly substituted isotopologues (e.g., $^{13}C^{18}O^{16}O^{16}O^{2-}$). For fundamental thermodynamic reasons, ^{13}C–^{18}O bonds in a carbonate mineral are more abundant in carbonates equilibrated at low than high temperatures (e.g. Schauble et al., 2006), and this distribution may be preserved over geologic time scales under favourable circumstances (Passey and Henkes, 2012; Stolper and Eiler, 2015). By precisely measuring the abundance of the multiply-substituted, mass-47, isotopologues in the CO_2 produced by acid digestion of a carbonate sample it is possible to constrain its original crystallisation temperature without making assumptions regarding the composition of parent waters. Full analytical techniques are provided in Supplementary Material S1.

A concern for clumped isotope thermometry with samples as old as those studied here is that they may have undergone solid-state reordering. In this process the abundance of clumped carbonate groups in the mineral changes in response to the breaking and reformation of bonds within the mineral lattice (e.g. Passey and Henkes, 2012). As a thermally activated process solid-state reordering will reset T_c if the sample is held at sufficiently high temperature for sufficiently long. Experimental studies suggest that samples formed at near-surface temperatures, such as those studied here, must be heated to ≥100 °C to induce measurable reordering on 100 Myr timescales (e.g. Passey and Henkes, 2012; Henkes et al., 2014; Stolper and Eiler, 2015). Based on the geological history of the study area (e.g. Robertson, 1977; Supplementary Material S3) we expected the carbonate clumped isotope distribution not to have been reset and, *a posteriori*, the low temperatures recorded by the clumped isotopes strongly support this.

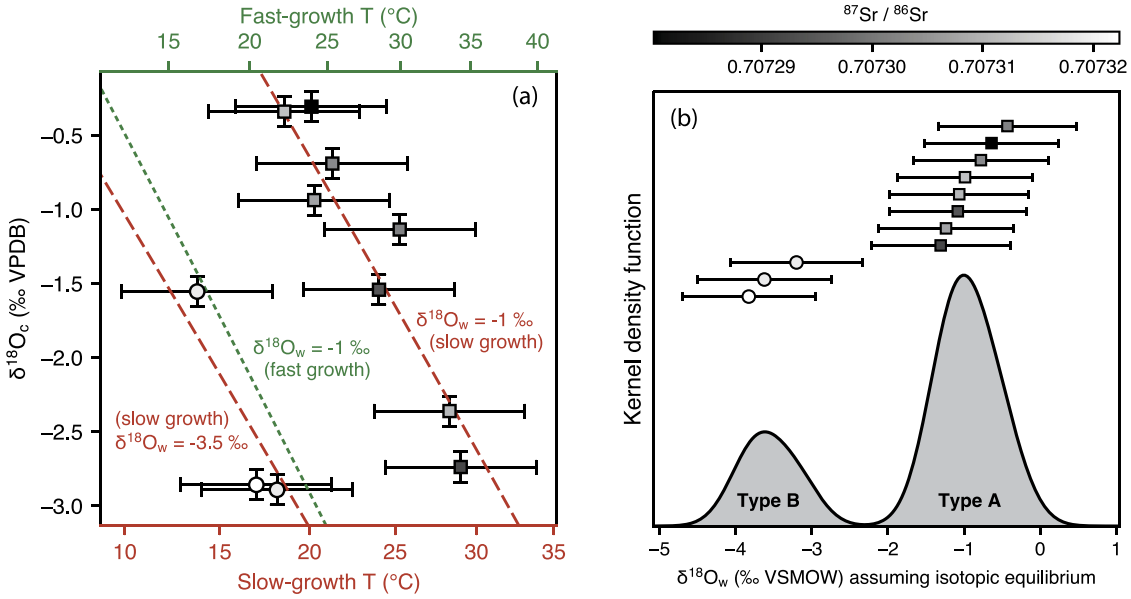

Fig. 3. (a) Δ_{47}-derived carbonate precipitation temperature plotted against carbonate $\delta^{18}O$, with 95% confidence limits. Eight of the eleven samples lie on the trend predicted for slow (equilibrium; red lines) growth from a water (subscript W) with $\delta^{18}O$ of −1‰ (as expected for Cretaceous seawater). The other three samples can be explained either as having grown from a fluid that was ~3‰ lighter or as having grown fast (green line), with kinetic isotope fractionation, from a fluid with $\delta^{18}O$ of −1‰; see text for discussion; (b) kernel density plots showing that the fluid O-isotope compositions calculated assuming equilibrium relationships (see text for discussion) fall into two distinct groups (type A and type B) that also have different, although similar, Sr-isotopic compositions (as shown by the symbol grey-scale in both part a and b).

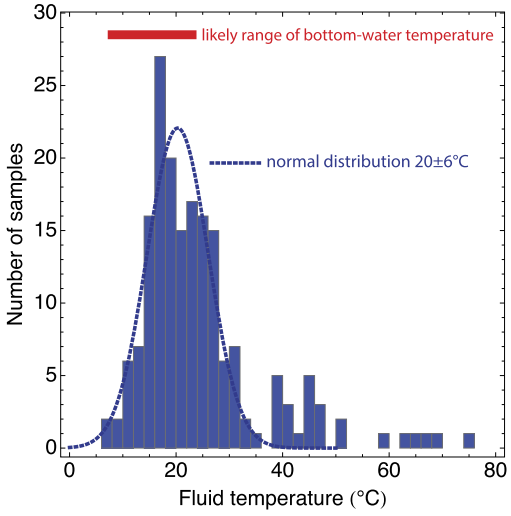

Fig. 4. Histogram of the calculated temperature of carbonate precipitation based on standard $\delta^{18}O$ thermometry for samples from the Troodos lavas ($n = 184$) assuming a fluid $\delta^{18}O$ of −1‰ using the Daëron et al. (in press) calibration (which is virtually identical to the Coplen (2007) thermometer). The blue curve shows the probability distribution for the average (20.3 °C) and standard deviation (5.8 °C) of all carbonate-derived temperatures <38 °C, which captures the distribution of the coolest 86% of the data. Higher temperatures are generally associated with deeper levels in the lavas, where the amount of carbonate is dramatically lower than at shallower crustal levels and fluid fluxes smaller, as well as in isolated regions interpreted as up-flow zones. The red bar shows the range in bottom water temperature during the first 20 Myrs after formation of the ophiolite (Friedrich et al., 2012), which is the main time interval of carbonate formation (e.g. Coogan and Gillis, 2018a).

4. Results

4.1. Calcite Δ_{47} and $\delta^{18}O$: aquifer fluid temperature and O-isotopic composition

The clumped isotope measurements yield average Δ_{47} ranging from 0.646 to 0.701‰. These data make it possible to estimate the temperature and oxygen-isotope composition of the water the calcite grew from provided we know the relationships between crystallisation temperature (T_c) and Δ_{47} and between T_c and $\alpha_{c/w}$ (the $^{18}O/^{16}O$ fractionation factor between calcite and water). Precisely calibrating the clumped-isotope carbonate thermometer has long remained challenging, at least in part because of significant inter-laboratory discrepancies. For this reason, and following earlier studies from other groups, we interpret our results based on calibration data sets obtained in the same laboratory used to analyse the samples (Peral et al., 2018; Daëron et al., in press).

Theoretical models suggest that both the relationship between T_c and Δ_{47} (Watkins and Hunt, 2015) and between T_c and $\alpha_{c/w}$ (e.g. Watkins et al., 2013) may be influenced by kinetic factors. Recently Daëron et al. (in press) have reported that inorganic carbonates that grew very slowly, and which are likely to have formed in oxygen-isotope equilibrium with their parent waters, define a different T_c–Δ_{47} relationship than faster growing biogenic calcite. Additionally, they found further support for the suggestion that at typical laboratory growth rates (e.g. those of Kim and O'Neil, 1997) kinetic effects lead to non-equilibrium calcite $\delta^{18}O$ (e.g. Coplen, 2007; Watkins et al., 2013; Levitt et al., 2018). They interpret the very slow-growing inorganic carbonates as recording equilibrium compositions and suggest that the faster growing calcites have slightly higher Δ_{47} and substantially lower $\delta^{18}O$ due to kinetic isotope effects associated with higher calcification rates (Coplen, 2007; Watkins et al., 2013; Daëron et al., in press). Because calcite in the upper oceanic crust forms over many millions of years (Staudigel and Hart, 1985; Coogan and Dosso, 2015), driven by the alkalinity generated by fluid–rock reactions, it seems likely that growth rates are generally slow in this setting. Thus, we initially use the slow-growth (equilibrium) calibrations reported by Daëron et al. (in press) to compute T_c from Δ_{47} and $\alpha_{c/w}$ from T_c (the latter being virtually identical to that of Coplen, 2007). This approach yields apparent crystallisation temperatures between 13.8 ± 2.1 and 29.0 ± 2.4 °C (±1 standard error; Fig. 3a). Using these temperatures and the equilibrium (slow-growth) relationship between $\alpha_{c/w}$ and T_c (Coplen, 2007; Daëron et al., in press) allows the $\delta^{18}O$ of the fluid the calcite grew from to be determined. This results in a strongly

bimodal distribution (Fig. 3b) of reconstructed water $\delta^{18}O_{VSMOW}$, with eight values tightly clustered around −1.0‰ (hereafter referred to as type A) and the remaining three around −3.5‰ (hereafter referred to as type B). Although different calibrations would lead to different absolute temperatures and fluid compositions, bimodality is an inherent feature of the data and would be present irrespective of the calibrations used.

In the Cretaceous, when the Troodos ophiolite formed, $\delta^{18}O_{SW}$ is thought to have been close to −1‰ due to the lack of ice sheets (e.g. Gregory and Taylor, 1981). Thus, the type A calcite can be explained as having grown slowly from a fluid with seawater-like $\delta^{18}O$. Such a model is consistent with the expectation that water-rock ratios are generally sufficiently high in off-axis hydrothermal systems that fluid–rock reactions are unlikely to substantially change the O-isotopic composition of the fluid. Clearly a different model is required to explain the type B calcites. Type B calcites are not obviously different to type A calcites in their C-isotopic composition, or Mg and Sr contents (Table S3). They also are from similar geological settings to the other samples (Fig. S2). The only independent characteristics that differentiate the type B calcites are that they have the three highest $^{87}Sr/^{86}Sr$ ratios (Fig. 3, Fig. S4) and the three lowest Δ_{47}-derived temperatures (Fig. 3), which is unlikely to result from chance alone.

The Sr-isotopic composition of carbonates precipitated during alteration of the lava section of the oceanic crust depends both on the Sr-isotopic composition of seawater at the time the carbonate grew and the amount of basaltic Sr dissolved out of the rock into the fluid (e.g. Staudigel and Hart, 1985). The Sr-isotopic compositions of the type B carbonates are analytically indistinguishable from one another (0.707319–0.707322) but are higher than any of the other samples we measured clumped isotopes on (0.707280–0.707311). Based on comparison with the seawater Sr-isotope curve of McArthur and Howarth (2004), the type B calcite either formed at or before 91.7 Ma, or at or after 89.1 Ma (Fig. S4). The former age matches the age of the ophiolite raising the possibility that these three carbonates precipitated very soon after ophiolite formation from a fluid with $^{87}Sr/^{86}Sr$ almost identical to seawater. We consider two hypotheses to explain the type B calcite: (i) growth from an isotopically very light fluid; and (ii) disequilibrium (fast) growth.

According to the first hypothesis, the type B calcite grew from a fluid with $\delta^{18}O$ of roughly -3.5 ± 0.3‰ which is substantially more ^{18}O depleted than the fluid the type A calcite are interpreted to have grown from and much lighter than Cretaceous seawater (Fig. 3). Fluid–rock reactions at low temperatures form minerals with high $\delta^{18}O$, leading to the lavas of the upper oceanic crust becoming isotopically heavy (Fig. 2), and hence the fluid in the lavas in the off-axis must be driven towards lower $\delta^{18}O$. Sufficient fluid–rock reaction, at a low water-to-rock ratio, could therefore lead to a fluid that was isotopically much lighter than seawater. Indeed, this model has been proposed for upper-oceanic crust carbonates from ODP Site 801 that coupled Δ_{47} and $\delta^{18}O$ data suggest grew from an isotopically light fluid (Stolper et al., 2016). However, the lavas from ODP Site 801 have a complex geological history, including off-axis volcanism, that led to carbonate formation at anomalously high temperatures (up to >60 °C; Alt and Teagle, 2003) that can only be maintained at low water-to-rock ratios. In contrast, both thermal and chemical constraints suggest that off-axis alteration normally occurs at high water-to-rock ratios (>1000; e.g. Coogan and Gillis, 2018a). Under these circumstances mass balance constraints mean that the bulk fluid cannot be driven to significantly lighter $\delta^{18}O$ than seawater.

Both thermal and chemical constraints require regional scale water-to-rock ratios in the lavas to be high. However, on a local scale the fluids could experience much smaller water-to-rock ratios. It is possible that this was the case for the fluid that the calcite in amygdales grew from because this fluid must have passed through a low-permeability rock to reach the vesicle. Is it possible that the fluid in vesicles had a much lower $\delta^{18}O$ than the bulk fluid in the lavas because of evolving in a local low-water-to-rock system? Three qualitative arguments suggest that this was not the case. First, all calcite $^{87}Sr/^{86}Sr$ are similar to that of late Cretaceous seawater indicating little modification of the fluid Sr-isotopic composition by rock dissolution (Fig. 3; Fig. S4). Since Sr-isotopes should be more strongly affected by rock dissolution than O-isotopes, little modification of the fluid O-isotopic composition is expected. Second, if fluid–rock reaction modified the fluid O-isotopic composition substantially then this should be seen most strongly in the calcite samples precipitated at higher temperatures because reaction rates increase with increasing temperature. Instead, type B samples grew at the lowest temperatures based on their Δ_{47} (Fig. 3). Third, a continuum of calcite compositions would be expected in this scenario rather than the bimodal distribution we observed (Fig. 3). As a further test of whether fluid–rock reaction could have driven the fluid that the type B calcite grew from to low $\delta^{18}O$ we applied the model of DePaolo (2006) to calculate the expected difference between the composition of fluid in vesicles and in the main fluid flow channels in the lava section (Supplementary material S4). This modelling also suggests that the fluid from which the calcite grew had a similar $\delta^{18}O$ to the bulk fluid within the lavas. Because both empirical arguments and quantitative modelling suggest the fluid in the amygdales is unlikely to be substantially lighter than the main formation fluid we discount hypothesis (i).

The alternative hypothesis (ii) to explain the type B calcite is that these samples did not grow at equilibrium and hence the equilibrium relationships between T_c and Δ_{47}, and between T_c and $\alpha_{c/w}$, used to calculate the fluid $\delta^{18}O$ are inappropriate (Daëron et al., in press). This is most likely to be the case if the type B calcite grew faster than the other calcite (e.g. Devriendt et al., 2017; Levitt et al., 2018; Watkins et al., 2014; Watkins and Hunt, 2015), however we lack independent estimates of growth rates and so cannot directly test this model. To investigate this we reprocessed the type B raw data using relationships Δ_{47} and T_c, and between T_c and $\alpha_{c/w}$, appropriate for fast-growing calcite (from Peral et al., 2018 and Kim and O'Neil, 1997, respectively). This increases the clumped-isotope temperatures for type B calcites by 3–4 °C, making them consistent with the lower range of type A temperatures, and brings the average predicted parental fluid $\delta^{18}O$ for type B calcites up to -1.4 ± 0.3‰ (1 SD). While potentially coincidental, the observation that this model leads to the same fluid O-isotope ratio as that derived from the slow-growth model for the type A calcites, and the same as expected for Cretaceous seawater, leads us to explore this "growth rate control" model further.

Two ways in which the calcite growth rate may have varied substantially between samples are if the initial $CaCO_3$ phase was not calcite and this subsequently recrystallised to form calcite, or if the rate of calcite precipitation changed over time after crustal accretion. In the former model if, for example, the original $CaCO_3$ phase was aragonite and this subsequently transformed to calcite it is plausible this transformation occurred rapidly leading to disequilibrium calcite growth. We have no reason to believe that recrystallisation of a precursor phase occurred and consider this a somewhat ad hoc, although plausible, explanation of the type B calcite. Our favoured model is that a change in calcite precipitation rate over time occurred. One might expect a change in the rate of calcite formation over time after crustal accretion because the reactions that drive calcite formation will be fastest when the crust is youngest and hence least altered. There are multiple possible causes of an age dependence of rock dissolution rates such as evolution of mineral surface roughness, accumulation of leached

layers and secondary precipitates and decreases in the reaction affinity driving dissolution (e.g. White and Brantley, 2003). Furthermore, observational support for a change in calcite formation rate with time after crustal accretion comes from model ages of calcite in the oceanic crust (Coogan and Dosso, 2015). If the type B calcite grew when the crust was young, and hence most reactive, the rate of alkalinity generation (and hence calcite precipitation) would have been the highest and hence calcite formation rates would also have been the highest. It is plausible that at this stage growth rates were sufficiently rapid so as to lead to disequilibrium calcite compositions. This model is consistent with the observation that the Sr-isotope ratios of the type B calcite match that of seawater at the time of ophiolite formation, but the type A calcite have lower $^{87}Sr/^{86}Sr$ (Fig. 3; Fig. S4).

In summary, eight out of eleven carbonates (type A) measured for clumped isotopes are most simply interpreted as having grown slowly in O-isotope (and clumped-isotope) equilibrium with a fluid with $\delta^{18}O$ of $-0.94 \pm 0.30‰$ (1 SD) at between 18.6 ± 2.2 and $29.0 \pm 2.4\,°C$ (Fig. 3). The other three samples (type B) could be explained by faster (disequilibrium) growth from a fluid with a similar O-isotope composition, with kinetic isotope effects leading to the different calcite compositions. Disequilibrium growth could occur during the initial stages of alteration of the lavas when the rocks are most reactive (e.g. contains copious, unarmored, glass) and hence the rate of calcite formation the highest.

If we assume that all of the carbonates grew from a fluid with $\delta^{18}O$ of approximately $-1‰$ then we can use standard O-isotope thermometry to determine the precipitation temperatures of all of the carbonates analysed for $\delta^{18}O$. The majority of the samples give temperatures of $20 \pm 6\,°C$ (1 SD) using the Daëron et al. (in press), or, equivalently, the Coplen (2007) relationship (Fig. 4). Bottom water temperature in the first 20 Myr after accretion of the Troodos crust, when most calcite forms (Coogan and Gillis, 2018a), was $\sim 15 \pm 7\,°C$ (Friedrich et al., 2012). Thus, the vast majority of calcite was precipitated at only $\sim 5\,°C$ above bottom water temperature. If the Kim and O'Neil (1997) thermometer was used instead the calculated temperatures decrease by 7 to 10 °C and ~15% of the samples have calculated precipitation temperatures $< 8\,°C$, which is lower than bottom water temperatures.

4.2. Silicate $\delta^{18}O$: extent of rock recrystallisation

Fig. 2 shows that the bulk-rock $\delta^{18}O$ of lavas from Cretaceous age oceanic crust is higher than that for late Cenozoic crust. Since $\delta^{18}O_{SW}$ was lower in the Cretaceous than late Cenozoic (due to the lack of ice sheets) this suggests that the extent of O-isotope exchange was greater in the Cretaceous. Because the temperature of fluid–rock reaction in the lavas is only slightly above that of bottom water (Figs. 3, 4) it seems likely that the higher bottom water temperature in the Cretaceous led to greater extents of O-isotope exchange between the lavas and ocean at that time than in the late Cenozoic. To further investigate O-isotope exchange between the lavas and ocean we collected data for whole-rock samples from the Troodos lavas that have also been analysed for their major element and Sr-isotopic compositions.

Whole-rock $\delta^{18}O$ generally decreases with depth in the lava pile in each of the four lava sections in the Troodos ophiolite studied here, from a maximum of ~26‰ down to a minimum of ~8‰ (Fig. 5a) compared to a fresh rock $\delta^{18}O$ of $\sim 5.8 \pm 0.5‰$ (Supplementary Material S3). The extent of enrichment in ^{18}O in the altered lavas correlates with the enrichment in K_2O (Fig. 5d) and depletion in both Na_2O (Fig. 5c) and CaO from the silicate portion of the rock (CaO_{sil}; Fig. 5b). Almost all of the silicate-hosted Ca in the original rock has been leached from the samples with the highest whole-rock $\delta^{18}O$. Whole-rock $\delta^{18}O$ and $^{87}Sr/^{86}Sr_{(i)}$ (the age corrected initial Sr-isotopic ratio) also correlate strongly (Fig. 5e). Samples with the highest $\delta^{18}O$ have $^{87}Sr/^{86}Sr_{(i)}$ similar to late Cretaceous seawater; i.e. these samples completely equilibrated their Sr-isotopic composition with seawater during low-temperature alteration. Overall these observations point to the extent of O-isotope enrichment being largely controlled by the extent of recrystallisation of the primary rock with complete recrystallisation leading to a bulk-rock $\delta^{18}O$ of ~26‰.

Most samples from the modern ocean basins that have been analysed for O-isotopes have not also been analysed for major elements and Sr-isotopes preventing us from determining whether the correlations observed in the Troodos samples are a general feature of all altered lavas. Two locations from which samples have been more systematically analysed are the adjacent DSDP Holes 417A, 417D and 418A (120 Myr old Atlantic crust) and ODP Hole 801C (156 Myr old Pacific crust). For these cores so-called composite samples have been analysed more extensively than individual samples generally are. Similar correlations of whole-rock O-isotopic composition and K_2O, Na_2O and CaO_{sil} contents and $^{87}Sr/^{86}Sr_{(i)}$ are observed in the composite samples from DSDP Sites 417A, 417D and 418A and, for K_2O and Na_2O, in Hole 801C (data are not available for the other species for this core) suggesting that these are general characteristics of altered upper oceanic crust (Fig. 5).

Major element exchange between the ocean and oceanic crust during low-temperature hydrothermal circulation acts as a source of alkalinity to the fluid or, in other words, as a sink of CO_2 from the ocean–atmosphere system (Spivack and Staudigel, 1994; Coogan and Gillis, 2013). The magnitude of the alkalinity source can be determined by charge balance between the bulk composition of an altered rock and an estimate of its protolith composition (e.g. Spivack and Staudigel, 1994). The alkalinity produced by each sample increases roughly linearly with the O-isotopic composition of the sample (Fig. 5f). Thus, greater extents of fluid–rock reaction in the upper oceanic crust lead to both greater extents of O-isotope exchange and greater CO_2 consumption. The extent of CO_2 consumption has previously been shown to correlate with bottom water temperature (Gillis and Coogan, 2011) and the greater extent of O-isotope exchange in Cretaceous lavas than late Cenozoic lavas (Fig. 2) suggests that this is also dependent on bottom water temperature.

Additional evidence for alteration of the lavas at low-temperatures is provided by three celadonite separates collected from void spaces in the lava pile in the Troodos ophiolite that have $\delta^{18}O$ of $21 \pm 1‰$ (Table 1). The consistency of their O-isotopic composition suggests precipitation from a fluid with a similar temperature and O-isotopic composition. Using the isotopic fractionation factor for glauconite (Fig. S2) and a fluid $\delta^{18}O$ of $-1‰$ this would reflect equilibrium at $\sim 16\,°C$. While the fractionation factor is not well enough known to have confidence in the exact temperature, it seems likely that the celadonites grew at temperatures little above that of bottom water consistent with constraints from calcite thermometry (Fig. 3; Fig. 4).

5. Discussion: the CO_2-cycle as a buffer on seawater $\delta^{18}O$

The data presented above suggest that: (i) off-axis hydrothermal alteration of the upper oceanic crust typically occurs at only $\sim 5\,°C$ above bottom water temperature, with the fluid O-isotopic composition remaining close to that of seawater (Fig. 3; Fig. 4); (ii) the extent of alteration and O-isotope exchange between the ocean and lavas depends on bottom water temperature (Fig. 2; Gillis and Coogan, 2011; Coogan and Gillis, 2018b); and (iii) the extent of O-isotope exchange and alkalinity generation are linked (Fig. 5f). Here we use these observations to constrain a model of the O-isotope evolution of seawater.

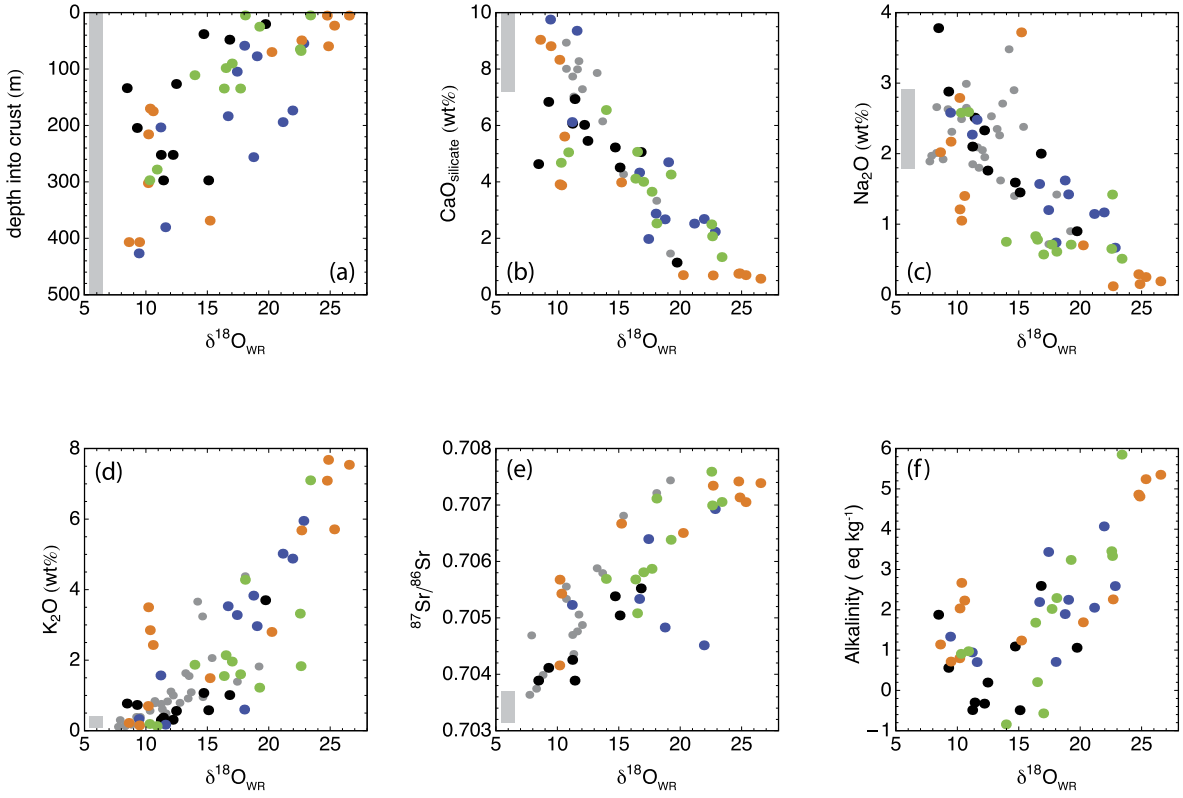

Fig. 5. Whole-rock $\delta^{18}O$ ($\delta^{18}O_{WR}$; VSMOW) v (a) depth, (b) CaO_{sil} (the whole-rock CaO content minus the CaO stored in carbonate minerals determined from the whole-rock CO_2 content assuming this is all housed in $CaCO_3$), (c) Na_2O, (d) K_2O, (e) Sr-isotope ratio (age corrected to 87 Myr), and (f) calculated alkalinity produced by fluid rock reaction (Coogan and Gillis, 2018b). Grey boxes show estimated fresh-rock compositions. The different colour symbols represent different sampling areas in the Troodos ophiolite: Green: Mitsero; Blue: Akaki; Orange: Politico; Black: Onophrious (see Fig. S2) and the smaller grey symbols in parts (b) to (e) are composite samples from DSDP Sites 417 and 418 (Staudigel et al., 1996) and ODP Hole 801C (Kelley et al., 2003; Alt, 2003). For Hole 801C the O-isotope data were corrected for intermixed sediment using the data in Alt (2003) and these samples are only shown for Na_2O and K_2O due to lack of data for other species. Whole-rock $\delta^{18}O$ are higher shallower in the crust and correlate with increased K_2O uptake from seawater, increased CaO and Na_2O release into seawater and increased $^{87}Sr/^{86}Sr$ exchange with seawater. Increased alkalinity production from the major element exchange between the crust and ocean also correlates with increased whole-rock $\delta^{18}O$ because both broadly reflect the extent of rock recrystallisation.

Table 1
Equations used in modelling the O-isotopic composition of seawater.

$\frac{d(\delta^{18}O_{SW})}{dt} = \frac{M^O_L(5.7-\delta^{18}O_{AL}) + M^O_D(5.7-\delta^{18}O_{AD}) + M^O_P(5.7-\delta^{18}O_{AP}) + M^O_{SS}(6-\delta^{18}O_{SS}) + M^O_{LM}(6-\delta^{18}O_{LM})}{m_o}$	Eq. S1
$\delta^{18}O_{AL} = \left(\delta^{18}O_{SW} + 30 - 0.25T_{BW}\right)F_{LT} + 5.7(1-F_{LT})$	Eq. S7
$\delta^{18}O_{AD} = 4.5 + 0.6\delta^{18}O_{SW}$	Eq. S3
$\delta^{18}O_{AP} = 5.1 + 0.2(\pm0.02)\delta^{18}O_{SW}$	Eq. S4
$\delta^{18}O_{SS} = \left(\delta^{18}O_{SW} - 3\right) + 20(\pm2) - 0.25(T_S - 15)$	Eq. S10
$\delta_{LM} = \delta^{18}O_{SW} + \left(\left(\frac{18030}{T_S+273}\right) - 32.43\right)$	Eq. S11
$F_{LT} = 0.07(\pm0.02)\mathrm{Exp}\left(\left(\frac{E_a^{SFW}}{R}\right)\left(\frac{1}{275} - \frac{1}{T_{BW}+273}\right)\right)$	Eq. S6
$M_{SS} = 2(\pm0.3)\times10^5\mathrm{Exp}\left(\left(\frac{E_a^{cont}}{R}\right)\left(\frac{1}{288} - \frac{1}{T_S+273}\right)\right)$	Eq. S9
$M_{LM} = M_{SS}/5(\pm1)$	Eq. S8

M^O: mass of oxygen added to the reservoir per unit time; L: lavas in seafloor weathering zone; AL: altered lavas; D: dikes; AD: altered dikes; P: plutonic rocks; AP: altered plutonic rocks; SS: newly formed silicate sediment; LM: carbonate sediment derived from silicate weathering; m_o: mass of oxygen in ocean; F_{LT}: fraction of lavas recrystallised during seafloor weathering. Surface temperature (T_S) is set such that sufficient alkalinity is generated via seafloor weathering and continental weathering to draw-down the CO_2 degassing flux prescribed in the model. Bottom water temperature (T_{BW}) = $T_S - 11$ (Krissansen-Totton and Catling, 2017); E_a: activation energy for seafloor weathering (SFW) and continental weathering ($cont$); Equation numbers refer to the supplementary material where these equations are described in detail.

The model of the O-isotope composition of seawater considers O-isotope fluxes associated with on- and off-axis hydrothermal alteration of the oceanic crust, continental chemical weathering, and the precipitation of sedimentary carbonates from the ocean (Table 1; Fig. S5). Each flux depends on the mass of material involved in the flux and the changes in O-isotopic composition between the protolith and final rock (Table 1; Eq. S1). For seafloor weathering and continental weathering the mass fluxes depend on global

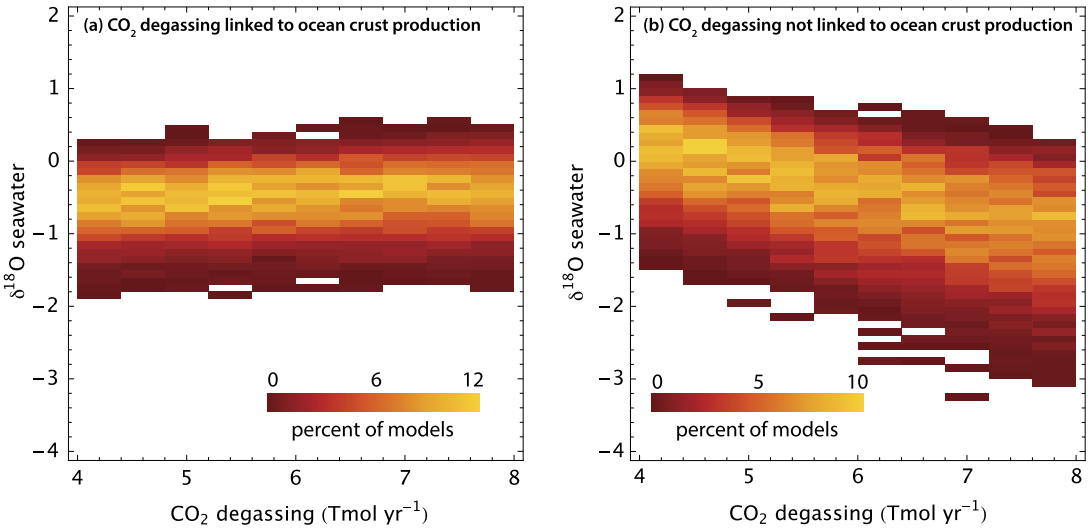

Fig. 6. Density plot of the results of Monte Carlo modelling of the steady-state $\delta^{18}O$ of seawater (VSMOW) as a function of changing solid Earth CO_2 degassing rate for the range of parameters given in Table S5. Part (a) has a 1:1 relationship between the rates of CO_2 degassing and oceanic crust formation and part (b) has no relationship between these parameters. The solid earth degassing rate shown is just that portion that is taken up as inorganic C and ignores the ~20% consumed as organic C; i.e. total degassing rates would be higher. For realistic ranges of Phanerozoic CO_2 degassing (as shown) the O-isotopic composition of the ocean (and continental ice) cannot vary much from the modern value if the rate of solid earth CO_2 degassing is tied to the rate of oceanic crustal production (a). If these are not linked, increased CO_2 degassing requires more low-temperature weathering reactions to drawdown the extra CO_2 into rocks and hence removes more ^{18}O from the ocean driving seawater isotopically lighter (b). Colour scale gives percent of model within a given range of $\delta^{18}O_{SW}$ for a given CO_2 degassing rate.

mean temperature such that higher temperatures lead to higher weathering fluxes. Surface temperature is set such that the prescribed CO_2 degassing flux is balanced by the CO_2 consumption via these two weathering fluxes; i.e. the O-isotope model is linked to the stabilising feedbacks of the long-term C-cycle. Such a link has also been recently suggested by Ryb and Eiler (2018). The fractionation of O-isotopes during high-temperature alteration of dikes and plutonic rocks at mid-ocean ridges is calculated based on the compiled data (Fig. 2). The fractionation of O-isotopes during seafloor weathering, continental weathering and carbonate sedimentation are dependent on global temperature. The solid earth CO_2 degassing flux can either be coupled with, or decoupled from, the rate of oceanic crustal formation. The values of many model parameters are not known precisely and so we use Monte Carlo simulations to explore how $\delta^{18}O_{SW}$ varies as a function of the controlling parameters.

The model results suggest that, irrespective of the uncertainty in the input parameters, the $\delta^{18}O$ of seawater should remain close to the modern value if the rate of solid earth degassing is closely tied to the rate of oceanic crust creation (Fig. 6a). In this scenario, increased CO_2 degassing leads (through increased surface temperature) to an increased weathering rate on both the seafloor and continents and increased carbonate sediment formation. In turn, because these processes operate at low temperatures, this increases the removal rate of ^{18}O from the ocean. However, this increased sink for ^{18}O is counterbalanced by the larger mass of dikes and plutonic rocks reacting with seawater on-axis at high-temperatures which increases the flux of ^{18}O into the ocean. This result is relatively insensitive to the activation energy for both seafloor and continental weathering. The dominant control on the scatter in model $\delta^{18}O_{SW}$ is the thickness of the sheeted dike complex (and to a lesser extent the plutonic complex) with models with thicker sheeted dike complexes having a larger flux of ^{18}O into the ocean from the dikes, and hence higher $\delta^{18}O_{SW}$. In the modern oceans the thickness of the sheeted dike complex depends on the depth of the magma reservoir feeding lava flows and is principally controlled by spreading rate. Global average spreading rates may have fluctuated over the Phanerozoic but are unlikely to have changed systematically. Further back in Earth history, if higher mantle heat loss was dissipated through faster spreading, average sheeted dike complexes may have been thinner perhaps reducing the flux of ^{18}O into the ocean.

It is possible that solid Earth CO_2 degassing has been decoupled from the rate of formation of new seafloor either during geologically brief periods (e.g. during formation of large igneous provinces) or if Earth's tectonic regime was substantially different in the past. In this scenario, all other things being equal, increased CO_2 degassing leads to an increase in the mass of low-temperature mineral formation required to balance the alkalinity budget of the ocean, and hence an increased sink for ^{18}O (whether in the upper oceanic crust or on the continents). This leads to a decrease in $\delta^{18}O_{SW}$ with increasing CO_2 degassing (Fig. 6b).

Over long periods of time models that closely link solid earth degassing rate and oceanic crustal production rate are probably more realistic than those that do not (e.g. Berner, 1991). Additionally, irrespective of whether the rates of solid earth CO_2 degassing and oceanic crust formation are linked, limited systematic variation in either parameter is expected over the Phanerozoic. This is because both are expected to be generally related to the secular cooling of the mantle, which has been limited over this time. Thus, it seems unlikely that the isotopic composition of seawater has increased systematically over the Phanerozoic by ~6‰ as has been suggested. Alternative models to explain the carbonate and chert $\delta^{18}O$ data for early Phanerozoic samples will probably have to be found. This conclusion is consistent with recent work using clumped isotope analysis of Phanerozoic carbonates (e.g. Came et al., 2007; Cummins et al., 2014; Finnegan et al., 2011; Henkes et al., 2018; Ryb and Eiler, 2018) that suggest that $\delta^{18}O_{SW}$ has not changed substantially over the Phanerozoic.

Our model reveals a problem in a currently popular hypothesis to explain the purported increase in $\delta^{18}O_{SW}$ over the Phanerozoic, that proposes that increased pelagic sedimentation reduced ingress of seawater into the upper oceanic crust, thus decreasing the extent of seafloor weathering over this time (Wallmann, 2004; Kasting et al., 2006; Jaffrés et al., 2007). This model does not account for the alkalinity balance. All other things being equal, decreased seafloor weathering would require increased continental weathering to balance the C-cycle. In turn, the removal of ^{18}O from the ocean would simply shift from the upper oceanic crust to continental margin sediments; this ^{18}O sink would not disappear

as would be required to drive a large increase in $\delta^{18}O_{SW}$ over the Phanerozoic.

The suggestion that the O-isotopic composition of seawater is unlikely to have changed much over the Phanerozoic is not new (e.g. Muehlenbachs and Clayton, 1976; Gregory and Taylor, 1981; Muehlenbachs, 1998) but our explanation for why this is the case differs significantly from most previous work. Previous models have commonly suggested that alteration of the oceanic crust buffers the O-isotopic composition of the ocean based on fixed extents of high- and low-temperature alteration driving the ocean to be ~6‰ lighter than the oceanic crust. Instead, we suggest that because many of the same processes control both the O-isotopic composition of seawater and the long-term carbon cycle, the feedbacks related to the latter prevent the O-isotopic composition of seawater changing dramatically, at least over the Phanerozoic.

5.1. Unravelling the history of $\delta^{18}O_{SW}$

Because clumped isotope analysis of seafloor carbonates from ophiolites appears to allow the O-isotopic composition of the deep ocean to be determined from ophiolite samples (Fig. 3), analysis of ophiolite-hosted carbonate may provide a mechanism to determine the long-term history of the O-isotopic composition of the deep ocean. This would avoid some of the uncertainties associated with similar studies using shallow marine carbonates (e.g., Came et al., 2007; Cummins et al., 2014; Finnegan et al., 2011; Henkes et al., 2018) where the water the carbonate precipitated from may not be representative of the average global ocean (e.g. Muehlenbachs, 1998). However, we caution that the low-temperature seafloor weathering of the lava section of the Troodos ophiolite is exceptionally preserved, and the samples studied here come from the best studied part of this ophiolite. Even with this context we see complexity in interpreting the data due to the apparent growth-rate control on the composition of some samples (Fig. 3). Using similar approaches on older, and less well-preserved, ophiolites will require very careful consideration of whether the material studied really preserves a record of the growth conditions.

6. Conclusions

Using both new and compiled isotope data for whole-rock samples and carbonates from the lava section of the oceanic crust we: (i) have confirmed that alteration of the lavas typically occurs at near bottom water temperature with the fluid flux being sufficient that only minor changes in the O-isotopic composition of the formation fluid generally occur; (ii) show that the extent of O-isotopic exchange between seafloor lavas and seawater correlates with the extent of exchange of other components including alkalinity generation and is greater when bottom water temperature is higher (Fig. 2; Fig. 5); and (iii) introduce a simple model for the O-isotopic evolution of seawater that links the O-isotope and C-cycles. In this model the O-isotopic composition of seawater cannot change substantially over time if the rate of CO_2 degassing from the solid earth is tied to the rate of spreading at mid-ocean ridges. This is because while increased oceanic crustal production leads to an increased flux of ^{18}O to the oceans through high-temperature alteration of dikes and plutonic rocks at mid-ocean ridges, this is counter balanced by an increased CO_2 flux requiring increased low-temperature weathering (of seafloor lavas and/or the continents) which provides an increased ^{18}O sink. A roughly invariant $\delta^{18}O_{SW}$ is thus an expected consequence of the required balance between CO_2 degassing and drawdown.

Acknowledgements

Two anonymous reviewers and editor Louis Derry are thanked for their comments which improved the manuscript. The Geological Survey of Cyprus is thanked for access to the field area and their ongoing interest in our work. Fred Longstaffe is thanked for the whole-rock O-isotope data, Janet Gabites for standard carbonate O-isotope analyses, and John McAuthur for providing his seawater Sr-isotope curve. Aerona Moore, Matt Pope, Michaella Yakimoski, Margo Ramsay, Hunter Markvoort and Sebastian Bichlmaier are thanked for help in picking the carbonates used in this study. The analytical facilities at LSCE benefited from financial support from: Région Ile-de-France; Direction des Sciences de la Matière du Commissariat à l'Energie Atomique; Institut National des Sciences de l'Univers, Centre National de la Recherche Scientifique; Universtité de Versailles/Saint-Quentin-en-Yvelines; and Plateforme Analytique Géosciences Paris Saclay (PANOPLY). LAC and KMG were funded through NSERC Discovery (5098 & 155396) and Accelerator grants. The manuscript was largely prepared while the authors were guests at the Institute of Marine Sciences in Barcelona.

Appendix A. Supplementary material

Supplementary material related to this article can be found online at https://doi.org/10.1016/j.epsl.2018.12.014.

References

Alt, J.C., 2003. Stable isotopic composition of upper oceanic crust formed at a fast spreading ridge, ODP Site 801. Geochem. Geophys. Geosyst. 4. https://doi.org/10.1029/2002GC000400.

Alt, J.C., Muehlenbachs, K., Honnorez, J., 1986. An oxygen isotopic profile through the upper kilometer of the oceanic crust, DSDP Hole 504B. Earth Planet. Sci. Lett. 80, 217–229.

Alt, J.C., Teagle, D.A.H., 2003. Hydrothermal alteration of upper oceanic crust formed at a fast-spreading ridge: mineral, chemical, and isotopic evidence from ODP Site 801. Chem. Geol. 201, 191–211.

Berner, R.A., 1991. A model for atmospheric CO_2 over Phanerozoic time. Am. J. Sci. 291, 339–376.

Came, R.E., Eiler, J.M., Veizer, J., Azmy, K., Brand, U., Weidman, C.R., 2007. Coupling of surface temperatures and atmospheric CO_2 concentrations during the Palaeozoic era. Nature 449, 198–201.

Coogan, L.A., Dosso, S.E., 2015. Alteration of ocean crust provides a strong temperature dependent feedback on the geological carbon cycle and is a primary driver of the Sr-isotopic composition of seawater. Earth Planet. Sci. Lett. 415, 38–46.

Coogan, L.A., Gillis, K.M., 2013. Evidence that low-temperature oceanic hydrothermal systems play an important role in the silicate–carbonate weathering cycle and long-term climate regulation. Geochem., Geophys. Geosyst. 14, 1771–1786.

Coogan, L.A., Gillis, K.M., 2018a. Low-temperature alteration of the seafloor: impacts on ocean chemistry. Annu. Rev. Earth Planet. Sci. 46, 21–45.

Coogan, L.A., Gillis, K.M., 2018b. Temperature dependence of chemical exchange during seafloor weathering: insights from the Troodos ophiolite. Geochim. Cosmochim. Acta 243, 24–41.

Coogan, L.A., Gillis, K.M., Pope, M., Spence, J., 2017. The role of low-temperature (off-axis) alteration of the oceanic crust in the global Li-cycle: insights from the Troodos ophiolite. Geochim. Cosmochim. Acta 203, 201–215.

Coplen, T.B., 2007. Calibration of the calcite-water oxygen isotope thermometer at Devils Hole, Nevada, a natural laboratory. Geochim. Cosmochim. Acta 71, 3948–3957.

Cummins, R.C., Finnegan, S., Fike, D.A., Eiler, J.M., Fischer, W.W., 2014. Carbonate clumped isotope constraints on Silurian ocean temperature and seawater $\delta^{18}O$. Geochim. Cosmochim. Acta 140, 241–258.

Daëron, M., Drysdale, R.N., Peral, M., Huyghe, D., Blamart, D., Coplen, T.B., Lartaud, F., Zanchetta, G., in press. Most Earth-surface calcites precipitate out of isotopic equilibrium. Nat. Commun.

DePaolo, D.J., 2006. Isotopic effects in fracture-dominated reactive fluid–rock systems. Geochim. Cosmochim. Acta 70, 1077–1096.

Devriendt, L.S., Watkins, J.M., McGregor, H.V., 2017. Oxygen isotope fractionation in the $CaCO_3$–DIC–H_2O system. Geochim. Cosmochim. Acta 214, 115–142.

Finnegan, S., Bergmann, K., Eiler, J.M., Jones, D.S., Fike, D.A., Eisenman, I., Hughes, N.C., Tripati, A.K., Fischer, W.W., 2011. The magnitude and duration of Late Ordovician/Early Silurian Glaciation. Science 331, 903–906.

Friedrich, O., Norris, R.D., Erbacher, J., 2012. Evolution of middle to Late Cretaceous oceans—a 55 m.y. record of Earth's temperature and carbon cycle. Geology 40, 107–110.

Fritz, P., 1971. Geochemical characteristics of dolomites and the ^{18}O content of Middle Devonian oceans. Earth Planet. Sci. Lett. 11, 277–282.

Gillis, K.M., Coogan, L.A., 2011. Secular variation in carbon uptake into the ocean crust. Earth Planet. Sci. Lett. 302, 385–392.

Gillis, K.M., Coogan, L.A., Brant, C., 2015. The role of sedimentation history and lithology on fluid flow and reactions in off-axis hydrothermal systems: a perspective from the Troodos ophiolite. Chem. Geol. 414, 84–94.
Gillis, K.M., Robinson, P.T., 1990. Patterns and processes of alteration in the lavas and dykes of the Troodos Ophiolite, Cyprus. J. Geophys. Res. 95, 21,521–21,548.
Gregory, R.T., Taylor, H.P., 1981. An oxygen isotope profile in a section of Cretaceous oceanic crust, Samail Ophiolite, Oman: evidence for $\delta^{18}O$ buffering of the oceans by deep (>5 km) seawater-hydrothermal circulation at mid-ocean ridges. J. Geophys. Res., Solid Earth 86, 2737–2755.
Henkes, G.A., Passey, B.H., Grossman, E.L., Shenton, B.J., Pérez-Huerta, A., Yancey, T.E., 2014. Temperature limits for preservation of primary calcite clumped isotope paleotemperatures. Geochim. Cosmochim. Acta 139, 362–382.
Henkes, G.A., Passey, B.H., Grossman, E.L., Shenton, B.J., Yancey, T.E., Pérez-Huerta, A., 2018. Temperature evolution and the oxygen isotope composition of Phanerozoic oceans from carbonate clumped isotope thermometry. Earth Planet. Sci. Lett. 490, 40–50.
Jaffrés, J.B.D., Shields, G.A., Wallmann, K., 2007. The oxygen isotope evolution of seawater: a critical review of a long-standing controversy and an improved geological water cycle model for the past 3.4 billion years. Earth-Sci. Rev. 83, 83–122.
Kasting, J.F., Howard, M.T., Wallmann, K., Veizer, J., Shields, G., Jaffrés, J., 2006. Paleoclimates, ocean depth, and the oxygen isotopic composition of seawater. Earth Planet. Sci. Lett. 252, 82–93.
Kelley, K.A., Plank, T., Ludden, J.N., Staudigel, H., 2003. Composition of altered oceanic crust at ODP Sites 801 and 1149. Geochem. Geophys. Geosyst. 4. https://doi.org/10.1029/2002GC000435.
Kim, S.-T., O'Neil, J.R., 1997. Equilibrium and non-equilibrium oxygen isotope effects in synthetic carbonates. Geochim. Cosmochim. Acta 61, 3461–3475.
Kirchner, T.M., Gillis, K.M., 2012. Mineralogical and strontium isotopic record of hydrothermal processes in the lower ocean crust at and near the East Pacific Rise. Contrib. Mineral. Petrol. 164, 123–141.
Krissansen-Totton, J., Catling, D.C., 2017. Constraining climate sensitivity and continental versus seafloor weathering using an inverse geological carbon cycle model. Nat. Commun. 8, 15423.
Lécuyer, C., Allemand, P., 1999. Modelling of the oxygen isotope evolution of seawater: implications for the climate interpretation of the $\delta^{18}O$ of marine sediments. Geochim. Cosmochim. Acta 63, 351–361.
Levitt, N.P., Eiler, J.M., Romanek, C.S., Beard, B.L., Xu, H., Johnson, C.M., 2018. Near equilibrium ^{13}C–^{18}O bonding during inorganic calcite precipitation under chemo-stat conditions. Geochem. Geophys. Geosyst. 19, 901–920. https://doi.org/10.1002/2017GC007089.
McArthur, J.M., Howarth, R.J., 2004. Strontium isotope stratigraphy. In: Gradstein, F.M., Ogg, J.G., Smith, A.G. (Eds.), A Geological Time Scale. Cambridge University Press, Cambridge, pp. 96–105.
Muehlenbachs, K., 1998. The oxygen isotopic composition of the oceans, sediment and the seafloor. Chem. Geol. 145, 263–273.
Muehlenbachs, K., Clayton, R.N., 1976. Oxygen isotope composition of the oceanic crust and its bearing on seawater. J. Geophys. Res. 81, 4365–4369.
Passey, B.H., Henkes, G.A., 2012. Carbonate clumped isotope bond reordering and geospeedometry. Earth Planet. Sci. Lett. 351–352, 223–236.
Peral, M., Daëron, M., Blamart, D., Bassinot, F., Dewilde, F., Smialkowskii, N., Isguder, G., Bonnin, J., Jorissen, F., Kissel, C., Michel, E., Riveiros, N.V., Waelbroeck, C., 2018. Updated calibration of the clumped isotope thermometer in planktonic and benthic foraminifera. Geochim. Cosmochim. Acta 239, 1–16.
Perry, E.C., 1967. The oxygen isotope chemistry of ancient cherts. Earth Planet. Sci. Lett. 3, 62–66.
Polat, A., Frei, R., Longstaffe, F.J., Woods, R., 2018. Petrogenetic and geodynamic origin of the Neoarchean Doré Lake Complex, Abitibi subprovince, Superior Province, Canada. Int. J. Earth Sci. 107, 811–843.
Robertson, A.H.F., 1977. Tertiary uplift history of the Troodos massif, Cyprus. GSA Bull. 88, 1763–1772.
Ryb, U., Eiler, J.M., 2018. Oxygen isotope composition of the Phanerozoic ocean and a possible solution to the dolomite problem. Proc. Natl. Acad. Sci. http://www.pnas.org/content/early/2018/06/06/1719681115.
Savin, S.M., Epstein, S., 1970. The oxygen and hydrogen isotope geochemistry of ocean sediments and shales. Geochim. Cosmochim. Acta 34, 43–63.
Schauble, E.A., Ghosh, P., Eiler, J.M., 2006. Preferential formation of ^{13}C–^{18}O bonds in carbonate minerals, estimated using first-principles lattice dynamics. Geochim. Cosmochim. Acta 70, 2510–2529.
Shields, G., Veizer, J., 2002. Precambrian marine carbonate isotope database: version 1.1. Geochem. Geophys. Geosyst. 3, 1–12.
Spivack, A.J., Staudigel, H., 1994. Low-temperature alteration of the upper oceanic crust and the alkalinity budget of seawater. Chem. Geol. 115, 239–247.
Staudigel, H., Hart, S.R., 1985. Dating of ocean crust hydrothermal alteration: strontium isotope ratios from Hole 504B carbonates and reinterpretation of Sr isotope data from Deep Sea Drilling Project Sites 105, 332, 417, and 418. In: Init. Rep. Deep Sea Drill. Proj., vol. 83, pp. 297–303.
Staudigel, H., Plank, T., White, B., Schimincke, H.-U., 1996. Geochemical fluxes during seafloor alteration of the basaltic upper oceanic crust: DSDP Sites 417 and 418. In: Subduction: Top to Bottom. American Geophysical Union, Washington, DC, pp. 19–38.
Stolper, A.D., Eiler, J.M., 2015. The kinetics of solid-state isotope-exchange reactions for clumped isotopes: a study of inorganic calcites and apatites from natural and experimental samples. Am. J. Sci. 315, 363–411.
Stolper, A.D., Antonelli, M.A., Ramos, D.S., Bender, M.L., Schrag, D.P., DePaolo, D.J., Higgins, J.A., 2016. Isotopic constraints on the formation of carbonates during low-temperature hydrothermal oceanic crust alteration. In: American Geophysical Union, Fall General Assembly 2016. Abstract PP22B-04.
Turchyn, A.V., Alt, J.C., Brown, S.T., DePaolo, D.J., Coggon, R.M., Chi, G., Bédard, J.H., Skulski, T., 2013. Reconstructing the oxygen isotope composition of late Cambrian and Cretaceous hydrothermal vent fluid. Geochim. Cosmochim. Acta 123, 440–458.
Veizer, J., Ala, D., Azmy, K., Bruckenschen, P., Buhl, D., Bruhn, F., Carden, G.A.F., Diener, A., Ebneth, S., Godderis, Y., Jasper, T., Korte, C., Pawellek, F., Podlaha, O.G., Strauss, H., 1999. $^{87}Sr/^{86}Sr$, $\delta^{13}C$ and $\delta^{18}O$ evolution of Phanerozoic seawater. Chem. Geol. 161, 59–88.
Veizer, J., Prokoph, A., 2015. Temperatures and oxygen isotopic composition of Phanerozoic oceans. Earth-Sci. Rev. 146, 92–104.
Walker, J.C.G., Lohmann, K.C., 1989. Why the oxygen isotopic composition of seawater changes with time. Geophys. Res. Lett. 16, 323–326.
Wallmann, K., 2004. Impact of atmospheric CO_2 and galactic cosmic radiation on Phanerozoic climate change and the marine delta O-18 record. Geochem. Geophys. Geosyst. 5. https://doi.org/10.1029/2003GC000683.
Watkins, J.M., Hunt, J.D., 2015. A process-based model for non-equilibrium clumped isotope effects in carbonates. Earth Planet. Sci. Lett. 432, 152–165.
Watkins, J.M., Hunt, J.D., Ryerson, F.J., DePaolo, D.J., 2014. The influence of temperature, pH, and growth rate on the $\delta^{18}O$ composition of inorganically precipitated calcite. Earth Planet. Sci. Lett. 404, 332–343.
Watkins, J.M., Nielsen, L.C., Ryerson, F.J., DePaolo, D.J., 2013. The influence of kinetics on the oxygen isotope composition of calcium carbonate. Earth Planet. Sci. Lett. 375, 349–360.
Weis, D., Kieffer, B., Maerschalk, C., Barling, J., de Jong, J., Williams, G.A., Hanano, D., Pretorius, W., Mattielli, N., Scoates, J.S., Goolaerts, A., Friedman, R.M., Mahoney, J.B., 2006. High-precision isotopic characterization of USGS reference materials by TIMS and MC-ICP-MS. Geochem. Geophys. Geosyst. 7. https://doi.org/10.1029/2006GC001283.
White, A.F., Brantley, S.L., 2003. The effect of time on the weathering of silicate minerals: why do weathering rates differ in the laboratory and field? Chem. Geol. 202, 479–506.

Supplementary Material

S1. Clumped isotope analytical protocols

A total of 80 clumped-isotope analyses (44 unknowns and 36 standards) were performed at the Laboratoire des Sciences du Climat et de l'Environnement (LSCE) using the equipment and procedures described by Peral et al. (2018). Carbonate samples weighing between 2.0 and 2.4 mg were dissolved in a common, stirred, 104 % phosphoric acid bath at 90 °C for 15 minutes. After cryogenic removal of water, the evolved CO_2 passed through a Porapak Q column (50/80 mesh, 1 m length, 2.1 mm ID) held at −20 °C under helium 6.0 flow (25 mL/min). CO_2 was then quantitatively recollected by cryogenic trapping, and transferred by gas expansion into an Isoprime 100 dual-inlet mass spectrometer equipped with six Faraday collectors (m/z 44 to 49). Each analysis took about 3 hours, during which sample gas and working reference gas were allowed to flow from matching, 10 mL reservoirs into the source, through a pair of fused silica capillaries (65 cm length, 110 μm ID). Every 20 minutes, gas pressures were adjusted to achieve a mass 44 current of 40 nA, with differences between sample and reference gas generally below 0.1 nA. Background currents were measured in all high-gain collectors (m/z 45 to 49) before and after each pressure adjustment, with gas flowing into the source, and are found to strongly correlate with the mass 44 current.

Background-corrected ion current values were processed using the IUPAC ^{17}O-correction parameters (Brand et al., 2010) to compute $\delta^{13}C_{VPDB}$, $\delta^{18}O_{VPDB}$ and "raw" Δ_{47} values for each analysis. The isotopic composition ($\delta^{13}C$, $\delta^{18}O$) of our working reference

CO_2 was computed based on nominal $\delta^{13}C_{VPDB}$ and $\delta^{18}O_{VPDB}$ values for carbonate standard ETH-3 ($\delta^{13}C_{VPDB}$ = 1.71 ‰, $\delta^{18}O_{VPDB}$ = -1.78 ‰, Bernasconi et al., 2018) and an oxygen-18 acid fractionation factor of 1.008176 (Das Sharma et al., 2002). Three carbonate standards, ETH-1 to ETH-3 (Meckler et al., 2014; Bernasconi et al., 2018), were then used to convert raw Δ_{47} to "absolute" Δ_{47} values, following the procedure described by Daëron et al. (2016). The nominal Δ_{47} values for these standards are those recomputed by Bernasconi et al. (2018) using IUPAC parameters: 0.258 ‰ for ETH-1, 0.256 ‰ for ETH-2 and 0.691 ‰ for ETH-3. Each of the eleven unknown samples was analyzed four times, and each replicate analysis was assigned an analytical error equal to the aggregate external Δ_{47} reproducibility for our three standards (0.016 ‰).

S2. Temperature dependence of relevant fractionation factors

Estimates of mineral-water O-isotope fractionation factors for different minerals that are commonly found in lavas altered in low-temperature, off-axis, hydrothermal systems are between ~20 and ~40‰ at typical alteration temperatures (Fig. S1). All minerals show similar temperature dependencies, with a mean (weighted by approximate mineral abundances) change in O-isotopic fractionation factor with changing alteration temperature of 0.25±0.02‰ $°C^{-1}$. This means that as ocean bottom water temperature changes the bulk fractionation factor between lavas altered at low temperatures and the ocean will also change. Late Cretaceous bottom water was ~15°C warmer than late Cenozoic bottom water (e.g. Friedrich et al., 2012) and this will have led to a ~4 ‰ smaller bulk O-isotope fractionation factor between secondary minerals and seawater in low-temperature, off-axis, hydrothermal systems at that time.

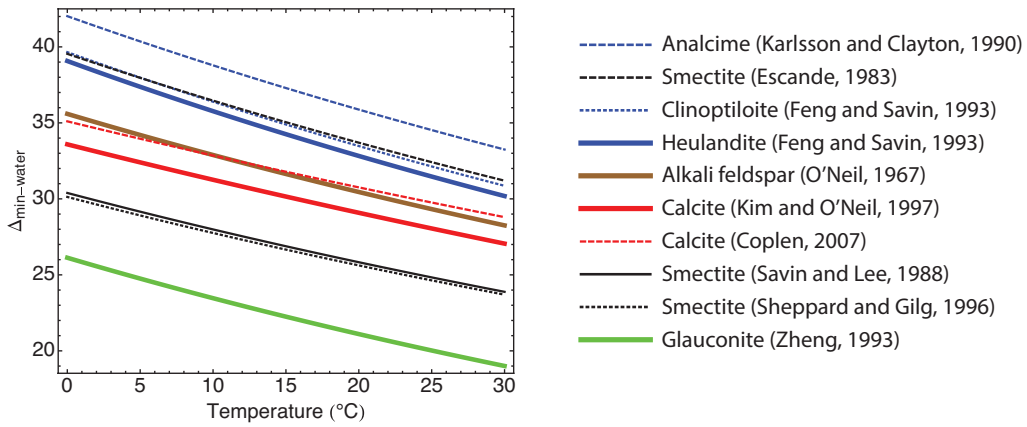

Fig. S1: Variation in fractionation factors as a function of temperature for common secondary minerals formed during off-axis hydrothermal alteration of ocean floor lavas.

S3. The study area

The study area is an almost 20 km section of the northern flank of the Troodos ophiolite between the villages of Kato Moni and Kambia (Fig. S2). The lavas of the ophiolite dip gently northwards and are overlain by seafloor sediments (largely carbonates). The lavas are well exposed in this area and carbonates from amygdales (or more rarely veins and vugs) have been collected from throughout the lavas across the entire area (Fig. S2). Temperatures derived from standard O-isotope thermometry demonstrate that there is a ~100-300 m thick upper region in which alteration temperature is approximately constant with depth, and below this alteration temperature increases with depth (Coogan and Gillis, 2018b). Whole-rock samples were collected along three surface traverses and from the CY1/1A drill cores (Fig. S2).

Fresh glass O-isotopic compositions for the Akaki area (5.8 ± 0.5, 1 SD; Rautenschlein et al., 1985) and a very fresh Troodos gabbro (5.6‰; Spooner et al., 1977) provide an estimate of the protolith O-isotopic composition in this area.

Sedimentation rates on the area of the Troodos ophiolite studied here were generally very slow with 10s of meters of calcareous sediment deposited over the first ~60 Myrs after ophiolite formation and then a more complex succession of reefal carbonates, evaporites and clastic sediments deposited in shallow marine environments since the mid-Miocene (Robertson, 1977). Maximum burial depths are thought to have been <<1 km suggesting that the ophiolite was not heated substantially post formation which is important for preservation of primary clumped isotope signatures.

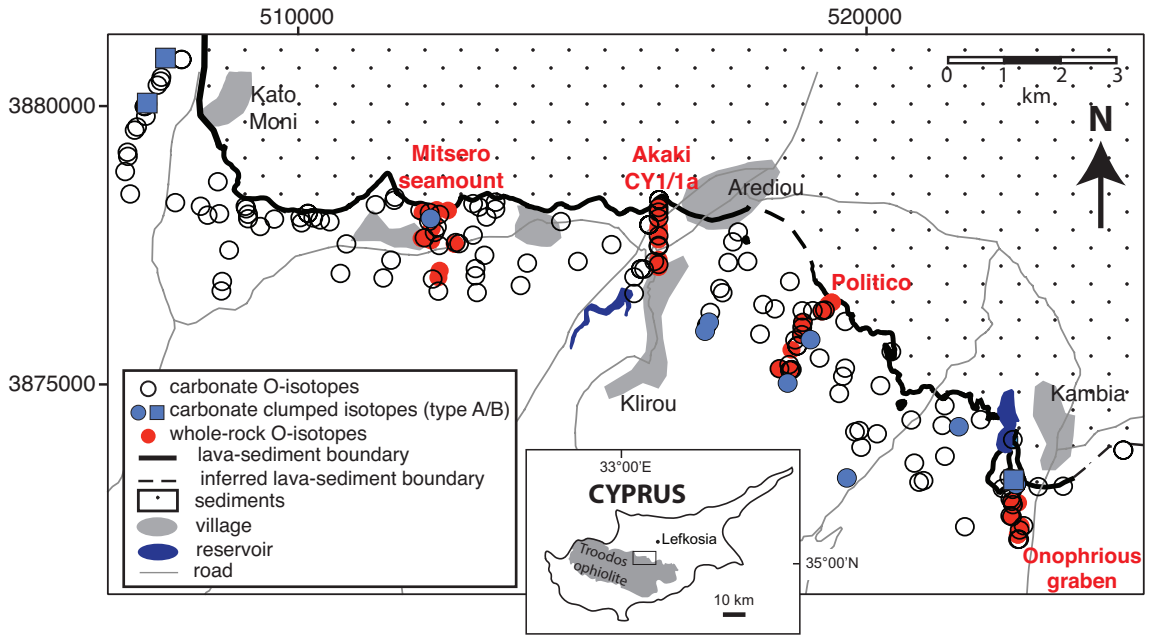

Figure S2: Map of the study area showing sample locations. CY1/1a drill core samples are projected to the surface for comparison with the other samples.

78

79 **S4. Modelling the O-isotopic composition of the fluid in vesicles**

80 Because most of our carbonate samples come from amygdales it is useful to
81 consider whether the fluid that these precipitated from is likely to have had a similar O-
82 isotopic composition to the main mass of fluid that flowed through the lava pile. To do
83 this we used the two-porosity model of DePaolo (2006). In this model fluid advects
84 through parallel fractures of a given separation and fluid-rock reactions occur in the rocks
85 between these fractures. In nature the channels are the margins of pillows and sheet flows
86 (i.e. separated by dm to m) and are not completely parallel but the model provides useful
87 insight into the overall process. The fluid in the rock matrix is assumed to be stationary
88 and exchange between this fluid and that in the channels occurs via diffusion. We
89 calculated the change in the O-isotopic composition of the fluid within the rock matrix as
90 a function of distance from the channel for a series of different channel separations, fluid-
91 rock reaction rates, and rock porosities (Fig. S3). For a range of plausible input
92 parameters (matrix porosity, channel separation and reaction rates), including more
93 extreme values than seem realistic (e.g. dissolution rates that would dissolve the entire
94 rock within 1 Myr), the fluid that carbonate amygdales would have grown from are
95 <0.2‰ lighter than the fluid in the channels. This scale of change is probably below the
96 resolution of our approach, and is negligible both in terms of interpreting the history of
97 the $\delta^{18}O$ of seawater and when calculating carbonate formation temperatures. The
98 interpretation that the fluid the amygdales grew from was generally very similar to the
99 bulk fluid within the lavas is further supported by the fact that amygdales are generally
100 concentrated in the rims of sheet flows and pillows and hence close to the conduits

through which fluid flows; i.e. in Fig S3 the modeled changes in fluid composition close the channel are the most relevant ones.

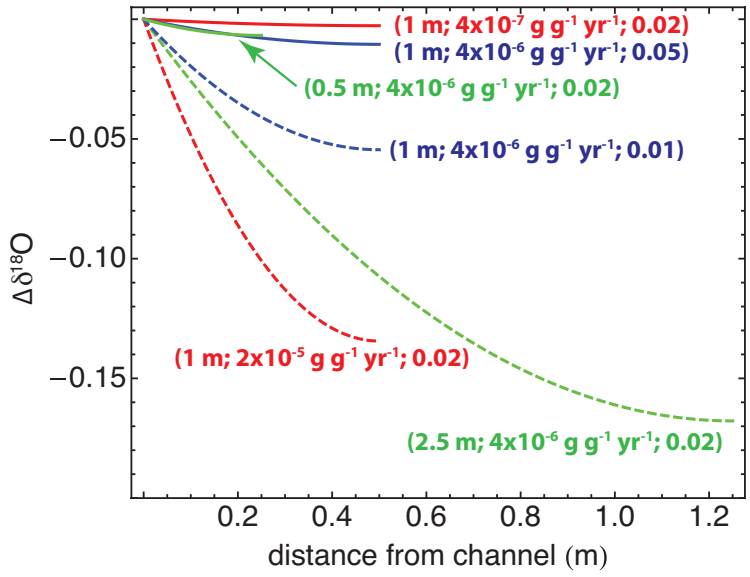

Figure S3. Results of modelling the difference in fluid O-isotopic composition between a stagnant fluid within the pores in the basalt matrix, that amygdale calcite could grow from, and the main fluid reservoir in the crust. The models assume that fluid flows in channels along the margins of pillow and sheet flows and O-isotopes are diffusively exchanged between this and stagnant fluid in the rock matrix (Eq. 25 of the dual porosity model of DePaolo, 2006). Model input: initial rock $\delta^{18}O = 5.7‰$; initial fluid $\delta^{18}O = 0‰$; $1000\ln(\alpha_{r/w}) = 25‰$; self diffusion coefficient of $H_2O = 0.024\ m^2\ yr^{-1}$ (Holz et al., 2000), for 10°C with a tortuosity correction of 0.5. Labels on curves: channel separation, dissolution rate, matrix porosity. Each pair of coloured curves has just one model parameter changed between them to illustrate the way in which that parameter affects the result.

118

119 **S5. Calcite Sr-isotopic compositions**

120 The Sr-isotopic composition of the calcite amygdales is controlled by both the Sr-
121 isotopic composition of seawater at the time they form and the amount of rock dissolved
122 into the fluid prior to calcite precipitation. Rock dissolution lowers the Sr-isotopic
123 composition of the fluid calcite grows from and thus calcite grown at any given time has
124 lower $^{87}Sr/^{86}Sr$ the greater the extent of fluid-rock reaction prior to calcite precipitation.
125 The Sr-isotopic composition of seawater changes over time and thus there is also
126 information about the age of the calcite crystal in their Sr-isotopic composition. For
127 example, the type B calcites have Sr-isotopic compositions of ~0.70732 and thus cannot
128 have formed in the time interval between ~89.5 and 91.5 Ma because seawater had a
129 lower Sr-isotopic composition than this during this interval (Fig. S4). The type B calcites
130 have higher $^{87}Sr/^{86}Sr$ than the type A calcites, and these match that of seawater at the time
131 of ophiolite formation (Fig. S4). Thus, one model for their formation is that they grew
132 immediately following ophiolite accretion from a fluid with little rock Sr in it. This model
133 is consistent with these calcite having the lowest formation temperatures (Fig. 3).

134

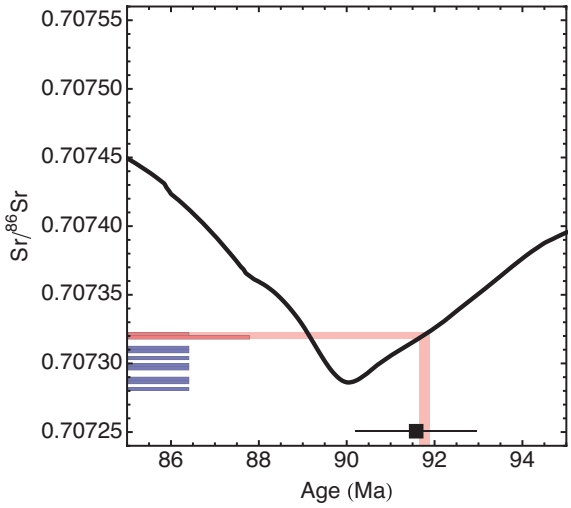

Fig. S4. Comparison of the Sr-isotopic composition of the calcite samples measured for their clumped isotopic composition (histogram on left; type A calcite shown in blue and type B in red) and the seawater Sr-isotope curve (black line; McAuthur and Howard, 2004). Also shown is the age of formation of the Troodos ophiolite (black square with error bar) based on a concordant zircon U-Pb age of 91.6±1.4 (Mukasa and Ludden, 1987) for a plagiogranite along strike (i.e. dike parallel) from our study area. The light red shading shows that the type B calcite could have formed very soon after ophiolite formation or after ~89.5 Ma but not in between these ages. These Sr-isotope data also allow us to rule out chemical exchange between the fluids the calcite amygdales grew from and the overlying sediments because the basal limestones overlying the ophiolite in the study area have much higher $^{87}Sr/^{86}Sr$ (>0.70775; and $\delta^{18}O$ between -1 and +1‰; Coogan and Gillis, unpub.) suggesting deposition ~20 Myr after ophiolite formation.

S6. Modelling the O-isotopic composition of seawater

The following describes the model used to evaluate the controls on seawater $\delta^{18}O$ and discusses the range of parameter values used in modelling $\delta^{18}O_{SW}$ and the assumptions made in constructing the model. Important features of the model (Fig. S5) that differentiate it from others in the literature include: (i) alkalinity is balanced such that the amount of weathering (combined seafloor and continental) is sufficient to generate the alkalinity needed to draw-down the CO_2 degassed from the solid earth that is not taken up as organic carbon (the organic C sink is ignored here as it does not affect the O-isotopic composition of seawater) – this is important because all weathering processes take up isotopically heavy oxygen; (ii) changes in surface and bottom water temperature are accounted for in determining the fractionation factor for O-isotopes during seafloor and continental weathering; and (iii) the role of low- and high-temperature alteration of the oceanic crust are calibrated against new compilations of natural sample data (Fig. 2), and better estimates of water-rock ratios, than previously used.

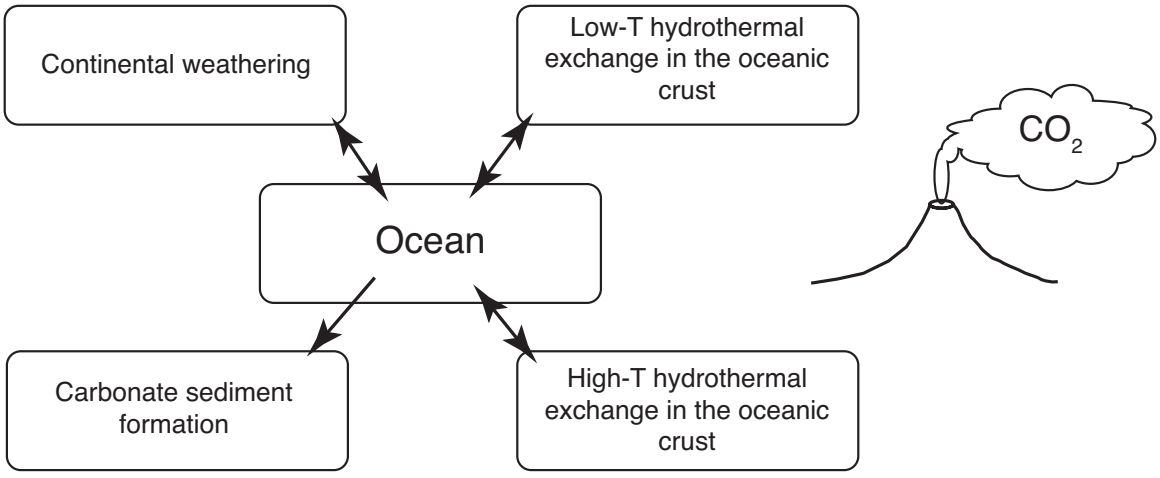

Figure S5. Schematic of the model used for determining the range of possible steady-state $\delta^{18}O_{SW}$. The model is driven by solid earth CO_2 degassing (schematically shown as a volcano) and includes O-isotope exchange (double-headed arrows) between the ocean and oceanic crust during high- and low-temperature hydrothermal circulation, O-isotope exchange during continental weathering (forming new silicate material that has equilibrated its O-isotopes with the exosphere) and carbonate sediment precipitation (single headed arrow) from the ocean.

S6.1. A simple model for seawater $\delta^{18}O$

The change in seawater $\delta^{18}O$ with time ($d(\delta^{18}O_{SW})/dt$; all O-isotope data are on SMOW scale throughout) is calculated from a simple model (Fig. S5) that accounts for O-isotope exchange during on- and off-axis hydrothermal circulation, continental weathering and carbonate precipitation:

$$\frac{d(\delta^{18}O_{SW})}{dt} = \frac{M_L^O(5.7 - \delta^{18}O_{AL}) + M_D^O(5.7 - \delta^{18}O_{AD}) + M_P^O(5.7 - \delta^{18}O_{AP}) + M_{SS}^O(6 - \delta^{18}O_{SS}) + M_{LM}^O(6 - \delta^{18}O_{LM})}{m_o}$$

Eq. S1

where, M^O = mass (M) of oxygen (O) added to the reservoir per unit time, L = lavas in the seafloor weathering zone, D = dikes, P = plutonics, AL = lavas altered by seafloor weathering, AD = altered dikes, AP = altered plutonics, SS = newly formed silicic sediments that have equilibrated their O-isotope with the exosphere (e.g. clays), LM = carbonate sediments, $\delta^{18}O_X = \delta^{18}O$ of unit X after alteration/weathering and m_o = mass of oxygen in the ocean (ocean mass held constant at 1.4×10^{21} kg throughout; 88% oxygen).

The fresh rocks are assumed to have $\delta^{18}O$ of 5.7‰ (oceanic crust) and 6‰ (continental crust) prior to exchange of O-isotopes with the hydrosphere.

S6.2. The on-axis high-temperature hydrothermal flux

In on-axis, high-temperature (≥400°C), hydrothermal systems fluid-rock reactions are expected to achieve a close approach to equilibrium O-isotope exchange between the fluid and rock. The relatively small variation in $\delta^{18}O$ of sheeted dikes (Fig. 2b), and even smaller variation when samples from within close proximity to one another are considered (Alt et al., 1996; Gillis et al., 2001), is consistent with a close approach to equilibrium and this is assumed here. Mass balance constrains the exchange of oxygen isotopes between seawater and the crust at elevated temperatures in a manner apparently not included in the model of Muehlenbachs (1998):

$$M_W^O \delta^{18}O_{SW} + M_R^O \delta^{18}O_{FR} = M_W^O (\delta^{18}O_{AR} - \Delta) + M_R^O \delta^{18}O_{AR} \quad \text{Eq. S2}$$

where, subscripts *W*, *R*, *FR* and *AR* are water, rock, fresh rock and altered rock respectively, and Δ is the difference in O-isotopic composition (‰) between the rock and fluid at the temperature of fluid-rock reaction (typically ≥400°C). This equation is solved separately for the sheeted dikes and plutonic rocks due to both their different average O-isotopic composition (Fig. 2) and different water-to-rock ratios.

The difference between the O-isotope composition of the average altered sheeted dike from young oceanic crust ($\delta^{18}O$ ~4.5‰; Fig. 2) and a typical modern high-temperature vent fluid ($\delta^{18}O$ ~ 0.8‰; data from Shanks, 2001) constrains Δ to be ~3.7‰

during alteration of the dikes. Using these values suggests a water-to-rock oxygen ratio of ~1.5. Substituting these values into Eq. S2, and assuming a fresh rock value of 5.7‰ and rearranging gives:

$$\delta^{18}O_{AD} = 4.5 + 0.6\delta^{18}O_{SW} \quad \text{Eq. S3}$$

where, AD = altered dikes. This is quite different to the result given by Muelenbachs (1998) in his Eq. 4 that appears to ignore the contribution of O from the dikes (i.e. it appears to assume a very high water-to-rock ratio in the dikes).

The O-isotopic composition of the average altered plutonic rock ($\delta^{18}O$ ~5.1‰; Fig. 2) is less shifted relative to the fresh rock than that of the average dike; unfortunately we do not have fluid compositions to directly compare with the altered plutonic rocks. The higher $\delta^{18}O$ of the plutonic rocks than dikes most likely reflects the smaller water-to-rock ratio within the plutonic section of the crust. The higher temperature of alteration in the plutonic section than dikes (e.g. Gillis, 1995; Manning et al., 1996) should lead to a smaller fractionation factor between the fluid and rock. Letting Δ range between 2.5 and 3 for plutonic rocks in Eq. S2, requires M_W^O/M_R^O to be between 0.23 and 0.28 to give $\delta^{18}O$ of altered gabbros of 5.1‰ with $\delta^{18}O_{SW}$ = 0‰. This leads to:

$$\delta^{18}O_{AP} = 5.1 + 0.2(\pm 0.02)\delta^{18}O_{SW} \quad \text{Eq. S4}$$

Compared to the dikes, the smaller water-to-rock ratio means that the composition of the plutonic rocks is less strongly influenced by the O-isotopic composition of seawater; however, the larger mass of plutonic rocks leads to dikes and plutonics having similar scales of importance in controlling the evolution of seawater $\delta^{18}O$.

S6.3. The off-axis low-temperature hydrothermal flux

In off-axis hydrothermal systems the extent of O-isotope exchange is dependent on the extent of recrystallization of the fresh rock (and consequent formation of secondary minerals) as well as on the O-isotopic composition of the secondary minerals formed. In the model the change in rock $\delta^{18}O$ in off-axis hydrothermal systems is calculated accounting for both the larger fraction of O-exchanged when bottom water is warmer (i.e. greater extent of recrystallization of the rock; Fig. 2) and the change in the fractionation factor with changing bottom water temperature (Fig. S1). The difference between the $\delta^{18}O$ of lavas altered in the Cretaceous (9.9-10.6‰ dependent on whether the arthimetic or geometric mean is used) and late Cenozoic (6.9-7.0‰; Fig. 2) is used to determine the change in the fraction of lavas replaced by low-temperature minerals during seafloor weathering (F_{LT}) with changing bottom water temperature. Data for samples from the modern ocean basins are used in an attempt to minimize sampling biases (i.e. comparing like with like). The end-member completely altered Cretaceous lava is assumed to have a $\delta^{18}O$ of 26% (Fig. 5) and the change in bottom water temperature (T_{BW}) relative to the modern is assumed to have been between 10 and 15°C (decreasing the fractionation factor by between 2.5 and 3.8‰; 3.1±0.7‰ in Eq. S5b). In doing this we assume a simple kinetic control on the extent of O-isotope exchange during

off-axis hydrothermal circulation (i.e., the extent of recrystallization of the rock) and determine the effective activation energy:

$$\frac{F_{LT}^{Cretaceous}}{F_{LT}^{Recent}} = Exp\left(\left(\frac{E_a^{SFW}}{R}\right)\left(\frac{1}{273+T_{BW}^{Recent}} - \frac{1}{273+T_{BW}^{Cretaceous}}\right)\right) \quad \text{Eq. S5a}$$

$$\frac{(10.25\pm0.35-5.7)/(26-5.7)}{(6.95\pm0.05-5.7)/(26-5.7+3.1\pm0.7)} = Exp\left(\left(\frac{E_a^{SFW}}{R}\right)\left(\frac{1}{275} - \frac{1}{287.5\pm2.5}\right)\right) \quad \text{Eq. S5b}$$

where R is the gas constant (8.314 J mol^{-1} K^{-1}); $F_{LT}^{Cretaceous}$ = fraction of primary minerals replaced by low-temperature minerals during seafloor weathering in Cretaceous lavas; F_{LT}^{Recent} = fraction of primary minerals replaced by low-temperature minerals during seafloor weathering in recent lavas. This leads to a range of activation energies for seafloor weathering (E_a^{SFW}) from 57 to 103 kJ mol^{-1} and this range is used in the modeling. These values are consistent with those determined from modelling Sr-isotope exchange (92 kJ mol^{-1}; Coogan and Dosso, 2015) and C-uptake by the crust (75 kJ mol^{-1}; Coogan and Gillis, 2018a) and the range of 53-97 kJ mol^{-1} derived from inverting a C-cycle model (Krissansen-Totton and Catling, 2017). While this gives the temperature dependence of the fraction of the lavas replaced at low temperature (F_{LT}) the absolute value of F_{LT} depends on whether the modern seafloor or ophiolite data is considered more representative. The former has the advantage of being derived from samples with MORB protolith compositions but the latter suffers less from sampling biases (e.g. poor recovery of the most altered material in drill cores). The range of possible values is encompassed by:

$$F_{LT} = 0.07(\pm 0.02) Exp\left(\left(\frac{E_a^{SFW}}{R}\right)\left(\frac{1}{275} - \frac{1}{273+T_{BW}}\right)\right) \quad \text{Eq. S6}$$

Where for model runs with high values of the pre-exponential the maximum activation energy for the run is reduced slightly (from 103 to 90 kJ mol^{-1} for the maximum pre-exponential of 0.09) to prevent F_{LT} exceeding 1, which is physically impossible.

The temperature dependence of the bulk fractionation factor for secondary minerals formed in off-axis hydrothermal systems is discussed in Section S2 and the value of 0.25‰ $°C^{-1}$ is used. Using the completely altered Cretaceous end-member bulk-rock $\delta^{18}O$ of 26‰ (assuming a bottom water temperature of 12°C and $\delta^{18}O^{SW}$ of -1‰) leads to:

$$\delta^{18}O_{AL} = (\delta^{18}O_{SW} + 30 - 0.25T_{BW})F_{LT} + 5.7(1 - F_{LT}) \quad \text{Eq. S7}$$

S6.4. Continental chemical weathering and carbonate sedimentation

The net effect of continental weathering of silicate material, and the associated diagenetic alteration of the sediments produced, can be thought of as the transformation of originally igneous rocks into a mixture of clastic sediments (composed of new minerals and clasts of the primary rock) along with chemical sediments formed from the dissolved load (dominantly carbonates). Taking a long-term river flux of ~$1x10^{16}$ g yr^{-1} ($150x10^6$ km^2 eroded at 24 m Myr^{-1}; Wilkinson, 2005) with 20% being new clastic silicate sediment (M_{SS}; g yr^{-1}) (with the remainder being recycled clasts and dissolved

299 load; Wallmann, 2001) gives $2x10^{15}$ g yr^{-1} of new clastic silicate sediment (that has
300 changed its O-isotopic composition) to which we arbitrarily assign an uncertainty of 15%.
301 The rate of new carbonate sediments formation (M_{LM}) is controlled by the rate of
302 alkalinity generation (at least that related to Ca and Mg release, see below) during
303 continental weathering (i.e. the dissolved load). Recycling of carbonate sediments is
304 ignored here because, on long timescales, this plays little role in the C-cycle (or O-cycle).
305 The present-day rate of CO_2 consumption by continental weathering can be estimated
306 from river chemistry. The chemistry of large rivers suggests ~$8.7x10^{12}$ to $10.6x10^{12}$ mol
307 yr^{-1} of CO_2 consumed (dependent on the assumptions about river Na contents) with ~60%
308 coming from Mg and Ca that can directly contribute to carbonate rocks and the other 40%
309 largely from K and Na that cannot (Gaillardet et al., 1999). The role of the alkalinity
310 carried by these alkali elements is unclear, with possibilities ranging from driving CO_2
311 consumption, for example if they are involved in converting plagioclase feldspar to alkali
312 feldspar, to driving CO_2 release if they are taken-up in reverse weathering reactions (e.g.
313 France-Lanord and Derry, 1997). It is also unclear how much additional CO_2 is consumed
314 by weathering of volcanic ocean islands (where Na and K are relatively minor
315 components) that are not included in the above estimate based on large rivers. Estimates
316 for CO_2 consumption in these settings are large, such as ~$0.9x10^{12}$ mol yr^{-1} of CO_2
317 consumed in tropical volcanic arcs (Shopka et al., 2011) to $3x10^{12}$ mol yr^{-1} of CO_2
318 consumed by weathering basaltic islands globally (Gaillardet et al., 1999). As a first
319 approximation we take 60% of the mean of the large river CO_2 consumption estimates
320 ($5.8x10^{12}$ mol yr^{-1}) and 100% of the mean of the basaltic island CO_2 consumption
321 estimates ($1.95x10^{12}$ mol yr^{-1}) giving a total CO_2 consumption rate of $7.75x10^{12}$ mol yr^{-1}

(±1.4 x10^{12}; 1σ). This is sufficient to form ~3.9x10^{12} moles of calcite (or ~3.9x10^{14} g yr^{-1} of calcite). Using the ratio of 2x10^{15} g yr^{-1} of new silicate sediment to 3.9x10^{14} g yr^{-1} of calcite derived from silicate alkalinity gives a roughly 5:1 ratio of new clastic sediment to new carbonate sediment. We assign an uncertainty of 20% using 5(±1):1 in the models giving:

$$M_{LM} = M_{SS}/5(\pm 1) \qquad \text{Eq. S8}$$

We use simple temperature-dependent kinetics to allow the rate of formation of new continental sediment, that has exchanged O-isotopes with the exosphere (M_{SS}; e.g. clays formed during weathering), to vary with surface temperature (T_S):

$$M_{SS} = 2(\pm 0.3) \times 10^{12} Exp\left(\left(\frac{E_a^{cont}}{R}\right)\left(\frac{1}{288} - \frac{1}{T_s+273}\right)\right) \qquad \text{Eq. S9}$$

which makes the rate of formation of sediments that have exchanged O-isotopes with the exosphere change as mean surface temperature diverges from 15°C. We explore a broad range of possible activation energies for silicate weathering on the continents (E_a^{cont}) of 20-80 kJ mol^{-1}.

Assuming that rainwater is on average 3‰ lighter than seawater (Muelenbachs, 1998; Rozanskial et al., 1993), and that the fluid to rock ratio during weathering is effectively infinite, the silicate weather products will have a bulk O-isotopic composition of:

$$\delta^{18}O_{SS} = (\delta^{18}O_{SW} - 3) + 20(\pm 2) - 0.25(T_S - 15) \quad \text{Eq. S10}$$

where 20±2‰ is the fractionation factor for typical new silicate sedimentary material suggested by Muehlenbachs (1998) with an uncertainty based on the scatter in clay compositions reported by Savin and Epstein (1970). In Eq. S10 the same temperature dependence for the isotopic fractionation factor as applied to seafloor weathering products is used (-0.25 per degree Celsius; Fig. S1) but this is calculated relative to a surface temperature of 15°C.

The O-isotopic composition of sedimentary carbonate rocks precipitated from seawater ($\delta^{18}O_{LM}$) is determined from:

$$\delta^{18}O_{LM} = \delta^{18}O_{SW} + \left(\left(\frac{18030}{T_S+273}\right) - 32.43\right) \quad \text{Eq. S11}$$

which uses the Kim and O'Neill (1997) calcite O-isotope thermometer (which is appropriate for rapidly grown calcite, which most sedimentary calcite probably is; Daëron et al., in review) and the surface temperature as most limestone is formed in near-surface conditions.

S6.5. Relating seafloor and continental weathering rates to solid earth CO_2 degassing through temperature

The mass of material formed during seafloor (*AL*) and continental weathering (*SS* and *LM*), and their O-isotopic compositions, depend on global temperature. Global temperature is linked in the model to the rate of CO_2 degassing from the solid Earth. As

already noted, we ignore CO_2 uptake as organic carbon, and thus CO_2 degassing rates considered here are proportionally lower than the total degassing rate. Any change in CO_2 degassing must be matched by a change in alkalinity production and hence CO_2 draw-down to maintain a steady-state exosphere C-content:

$$R\mathrm{CO}_2 = \frac{ALK_{SFW}}{2} + \frac{ALK_{cont}}{2} \qquad \text{Eq. S12}$$

Where $R\mathrm{CO}_2$ = the rate of degassing of CO_2 from the solid earth (mol yr^{-1}) excluding that portion that is buried as organic carbon; ALK = alkalinity production rate during seafloor weathering (SFW) and continental weathering ($cont$; corrected for that portion of the alkalinity associated with Na and K that does not result in carbonate rock production as discussed above). The alkalinity generation (eq yr^{-1}) from seafloor weathering is taken from Fig. 5f ($ALK_{SFW} = M_{AL}(4.02F_{LT})$; where M_{AL} is the mass production rate of lava that undergoes seafloor weathering (which is linked to bottom water temperature through Eq. S6). The alkalinity generation from continental weathering is simply $2M_{LM}/100$ where 100 is the molecular weight of calcite and 2 is the equivalents consumed in forming calcite. Surface temperature is set to the value required to satisfy Eq. S12 given the other model parameters.

386

387 **References for supplementary material**

388 Alt, J.C., Teagle, D.A.H., Bach, W., Halliday, A.N., Erzinger, J., 1996. Stable and
389 strontium isotopic profiles through hydrothermally altered upper oceanic crust, hole
390 504B, in: Alt, J.C., Kinoshita, H., Stokking, L., Michael, P. (Eds.), Proc. ODP, Sci.
391 Results. V. 148, p 57-69, ODP, College Station, Texas.

392 Bernasconi, S. M., I. A. Müller, K. D. Bergmann, S. F. M. Breitenbach, A. Fernandez, D.
393 A. Hodell, A. N. Meckler, I. Millan, M. Ziegler. 2018. Reducing uncertainties in
394 carbonate clumped isotope analysis through consistent carbonate-based
395 standardization. Geochemistry, Geophysics, Geosystems, 9, 2895–2914.
396 https://doi.org/10.1029/2017GC007385.

397 Brand W. A, Assonov S. S., Coplen T. B., 2010. Correction for the ^{17}O interference in
398 $\delta(^{13}C)$ measurements when analyzing CO_2 with stable isotope mass spectrometry
399 (IUPAC Technical Report) . Pure Appl. Chem. 82(8), pp. 1719-1733.

400 Coogan, L.A., Dosso, S., 2012. An internally consistent, probabilistic, determination of
401 ridge-axis hydrothermal fluxes from basalt-hosted systems. Earth Planet. Sci. Lett.
402 323, 92–101.

403 Coogan, L.A., Dosso, S.E., 2015. Alteration of ocean crust provides a strong temperature
404 dependent feedback on the geological carbon cycle and is a primary driver of the Sr-
405 isotopic composition of seawater. Earth Planet. Sci. Lett. 415, 38–46.

406 Coogan, L.A., Gillis, K.M., 2018. Low-Temperature Alteration of the Seafloor: Impacts
407 on Ocean Chemistry. Annu. Rev. Earth Planet. Sci. 46, 21-45.

408 Coplen, T.B., 2007. Calibration of the calcite-water oxygen isotope thermometer at
409 Devils Hole, Nevada, a natural laboratory. Geochim. Cosmochim. Acta 71, 3948–
410 3957.
411 Daëron, M., Drysdale, R.N., Peral, M., Huyghe, D., Blamart, D., Coplen, T.B., Lartaud,
412 F., Zanchetta, G. (in review) Most Earth-surface calcites precipitate out of isotopic
413 equilibrium, Nature communications.
414 Daëron, M., Blamart, D., Peral, M., Affek, H.P., 2016. Absolute isotopic abundance
415 ratios and the accuracy of Δ47 measurements. Chem. Geol. 442, 83–96.
416 Das Sharma, S., Patil, D.J., Gopalan, K., 2002. Temperature dependence of oxygen
417 isotope fractionation of CO_2 from magnesite-phosphoric acid reaction. Geochim.
418 Cosmochim. Acta 66, 589–593.
419 DePaolo, D.J., 2006. Isotopic effects in fracture-dominated reactive fluid-rock systems.
420 Geochim. Cosmochim. Acta 70, 1077–1096.
421 Escande, M.A., 1983. Echangeabilite et fractionnment isotopique de l'oxygene des
422 smectites magnesiennes de syntheses. Etablissement d'un geothermometre. Univ. de
423 Paris-Sud, Centre d'Orsay, Paris, France.
424 Feng, X., Savin, S.M., 1993. Oxygen isotope studies of zeolites—Stilbite, analcime,
425 heulandite, and clinoptilolite: II. Kinetics and mechanisms of isotopic exchange
426 between zeolites and water vapor. Geochim. Cosmochim. Acta 57, 4219–4238.
427 France-Lanord, C., Derry, L.A., 1997. Organic carbon burial forcing of the carbon cycle
428 from Himalayan erosion. Nature 390, 65–67.

429 Friedrich, O., Norris, R.D., Erbacher, J., 2012. Evolution of middle to Late Cretaceous
430 oceans—A 55 m.y. record of Earth's temperature and carbon cycle. Geol. 40, 107–
431 110.
432 Gillis, K.M., 1995. Controls on hydrothermal alteration in a section of fast-spreading
433 oceanic crust. Earth Planet. Sci. Lett. 134, 473–489.
434 Gillis, K.M., Muehlenbachs, K., Stewart, M., Gleeson, T., Karson, J., 2001. Fluid flow
435 patterns in fast-spreading East Pacific Rise crust exposed at Hess Deep. J. Geophys.
436 Res. 106, 26,311-326,329.
437 Holz, M., Heil, S.R., Sacco, A., 2000. Temperature-dependent self-diffusion coefficients
438 of water and six selected molecular liquids for calibration in accurate 1H NMR PFG
439 measurements. Phys. Chem. Chem. Phys. 2, 4740–4742.
440 Karlsson, H.R., Clayton, R.N., 1990. Oxygen isotope fractionation between analcime and
441 water: An experimental study. Geochim. Cosmochim. Acta 54, 1359–1368.
442 Kim, S.-T., O'Neil, J.R., 1997. Equilibrium and nonequilibrium oxygen isotope effects in
443 synthetic carbonates. Geochim. Cosmochim. Acta 61, 3461–3475.
444 Krissansen-Totton, J., Catling, D.C., 2017. Constraining climate sensitivity and
445 continental versus seafloor weathering using an inverse geological carbon cycle
446 model. Nat. Commun. 8, 15423, doi: 10.1038/ncomms15423.
447 Manning, C., Weston, P.E., Mahon, K.I., 1996. Rapid high temperature metamorphism of
448 the East Pacific Rise gabbros from Hess Deep. Earth Planet. Sci. Lett. 144, 123–132.
449 McArthur, J. M., & Howarth, R. J. (2004). Strontium Isotope Stratigraphy. In F. M.
450 Gradstein, J. G. Ogg, & A. G. Smith (Eds.), *A Geological Time Scale* (pp. 96–105).
451 Cambridge: Cambridge University Press.

452 Meckler A.N., Ziegler, M., Millan, M.I., Breienbach, S.F.M., Bernasconi, S.M. 2014,
453 Long-term performance of the Kiel carbonate device with a new correction scheme
454 for clumped isotope measurements. Rapid Commun. Mass Spectrom. 28, 1705–
455 1715.
456 Mukasa, S.B., Ludden, J.N., 1987. Uranium-lead isotopic ages of plagiogranites from the
457 Troodos ophiolite, Cyprus, and their tectonic significance. Geology 15, 825–828.
458 O'Neil, J.R., Taylor, H.P., 1967. The oxygen isotope cation exchange chemistry of
459 feldspars. Am. Min. 52, 1414–1437.
460 Rautenschlein, M., Jenner, G.A., Hertogen, J., Hofmann, A.W., Kerrich, R., Schmincke,
461 H.-U., White, W.M., 1985. Isotopic and trace element composition of volcanic
462 glasses from the Akaki Canyon, Cyprus: implications for the origin of the Troodos
463 ophiolite. Earth Planet. Sci. Lett. 75, 369–383.
464 Robertson, A.H.F., 1977. Tertiary uplift history of the Troodos massif, Cyprus. GSA
465 Bull. 88, 1763–1772.
466 Savin, S.M., Epstein, S., 1970. The oyxgen and hydrogen isotope geochemistry of ocean
467 sediments and shales. Geochim. Cosmochim. Acta 34, 43–63.
468 Savin, S.M., Lee, M., 1988. Isotopic studies of hydrous phyllosilicates, in: Bailey, S.W.
469 (Ed.), Reviews in Mineralogy 19: Hydrous Phyllosilicates (Exclusive of Micas). pp.
470 189–233.
471 Schopka, H.H., Derry, L.A., Arcilla, C.A., 2011. Chemical weathering, river
472 geochemistry and atmospheric carbon fluxes from volcanic and ultramafic regions on
473 Luzon Island, the Philippines. Geochim. Cosmochim. Acta 75, 978–1002.

474 Shanks, W.C., 2001. Stable isotopes in seafloor hydrothermal systems, in: Valley, J.W.,
475 Cole, D.R. (Eds.), Stable Isotope Geochemistry. Mineralogical Society of America,
476 pp. 469–526.
477 Sheppard S M F, Gilg H A, 1996. Stable Isotope Geochemistry of Clay Minerals. Clay
478 Miner. 31, 1-24.
479 Spooner, E.T.C., Chapman, H.J., Smewing, J.D., 1977. Strontium isotopic contamination
480 and oxidation during ocean floor hydrothermal metamorphism of the ophiolitic rocks
481 of the Troodos Massif, Cyprus. Geochim. Cosmochim. Acta 41, 873–890.
482 White, R.S., McKenzie, D., O'Nions, R.K., 1992. Oceanic Crustal Thickness From
483 Seismic Measurements and Rare Earth Element Inversions. Jour. Geophys. Res. 97,
484 19,619-19,715.
485 Zheng, Y.-F., 1993. Calculation of oxygen isotope fractionation in hydroxyl-bearing
486 silicates. Earth Planet. Sci. Lett. 120, 247–263.
487
488
489
490

Supplementary Tables

Table S1: Whole-rock compositions of lavas from the Troodos ophiolite

Table S2: Carbonate $\delta^{18}O$ compositions for samples from the lavas in the Troodos ophiolite

Table S3: Carbonate clumped isotope data for samples from the lavas in the Troodos ophiolite

Table S4: Sources of data used in constructing Fig. 2

Table S5: Symbol definitions and range of model parameters explored in modeling $\delta^{18}O_{SW}$

Table S5: Symbol definitions and range of model parameters explored in modeling $\delta^{18}O_{SW}$

Parameter	Symbol (units)	Minimum	Maximum[a]
O-isotopic composition of seawater	$\delta^{18}O_{SW}$		
O-isotopic composition of A	$\delta^{18}O_A$		
time	t (Myr)		
rate of CO_2 degassing (ignoring CO_2 subsequently drawn-down into organic C)	RCO_2 (mol yr^{-1})	$4x10^{12}$	$8x10^{12}$
thickness of lavas altered during seafloor weathering	T_L (m)	100	500
thickness of dikes	T_D (m)	750	1500
thickness of plutonics	T_P (m)	3000	5000
area rate of formation of new oceanic crust	A (km^2 yr^{-1})	2	4
density of lavas	ρ_L (kg m^{-3})	2500	
density of dikes	ρ_D (kg m^{-3})	2800	
density of plutonics	ρ_P (kg m^{-3})	3000	
rate of formation of lava that undergo seafloor weathering	M_L (kg Myr^{-1}) [b]	$A.T_L.\rho_L$	
rate of formation of dikes	M_D (kg Myr^{-1}) [b]	$A.T_D.\rho_D$	
rate of formation of plutonic rocks	M_P (kg Myr^{-1}) [b]	$A.T_P.\rho_P$	
rate of formation of new silicate sediments that have modified O-isotopic compositions (e.g. clays)	M_{SS} (kg Myr^{-1})		
rate of formation of carbonate sediments	M_{LM} (kg Myr^{-1})	$M_{SS}/6$	$M_{SS}/4$
oxygen in reservoir X	X^O		
mass of O in the ocean	m_o (kg)	$1.23x10^{21}$	$1.23x10^{21}$
fraction of the lavas recrystallized at low temperature	F_{LT}		
global mean surface temperature	T_S (°C)		
global mean bottom water temperature	T_{BW} (°C)	T_S - 11	
activation energy for seafloor weathering	E_a^{SFW} (kJ mol^{-1})	57	103
activation energy for continental weathering	E_a^{Cont} (kJ mol^{-1})	20	80

[a]Ranges of values are selected to span reasonable values for the Phanerozoic and are not meant to represent any specific time periods or conditions. Thickness of lavas, dikes and plutonics are from Coogan and Gillis (2018b), Coogan and Dosso (2012) and White et al. (1992) respectively, with the lower limit on the thickness of the plutonics based on assuming only the upper part of the plutonic section is hydrothermally altered.

[b]superscript O indicates mass of oxygen associated with these rocks